

Working Paper

Adaptive Robust Optimization for European Electricity System Planning Considering Regional Dunkelflaute Events

* Maximilian Bernecker (BTU Cottbus-Senftenberg), maximilian.bernecker@b-tu.de

Smaranda Sgarciu (BTU Cottbus-Senftenberg), smaranda.sgarciu@b-tu.de

Xiaoming Kan (Chalmers University of Technology) kanx@chalmers.se

Mehrnaz Anvari (Fraunhofer) (Fraunhofer SCAI), mehrnaz.anvari@scai.fraunhofer.de

Igor Riepin (TU Berlin), igor.riepin@tu-berlin.de

Felix Müsgens (BTU Cottbus-Senftenberg), felix.muesgens@b-tu.de

* Corresponding author.

E-mail address: maximilian.bernecker@b-tu.de (M. Bernecker)

Keywords: Renewable electricity system, Extreme weather events, Adaptive robust optimization, Long-term planning, Power generation, Transmission expansion

Abstract

The expansion of wind and solar power is driving the European energy system transformation, thereby also driving our reliance on this weather-dependent resources. Integrating renewable scarcity events into long-term planning has therefore become essential. This study demonstrates how worst-case regional renewable scarcity events - such as the *Dunkelflaute*, prolonged periods of low wind and solar availability - can be incorporated endogenously into the planning of a weather-robust, interconnected energy system. We develop a capacity expansion model for a fully decarbonized European electricity system using an adaptive robust optimization framework which incorporates multiple extreme weather realizations within a single optimization run. Results show that system costs rise nonlinearly with the geographic extent of these events: a single worst-case regional disruption increases costs by 9%, but broader disruptions across multiple regions lead to much sharper increases, up to 51%. As *Dunkelflaute* conditions extend across most of Europe, additional cost impacts level off, with a maximum increase of 71%. The optimal technology mix evolves with the severity of weather stress: while renewables, batteries, and interregional transmission are sufficient to manage localized events, large-scale disruptions require long-term hydrogen storage and load shedding to maintain system resilience. Central European regions, especially Germany and France, emerge as systemic bottlenecks, while peripheral regions bear the cost of compensatory overbuilding. These findings underscore the need for a coordinated European policy strategy that goes beyond national planning to support cross-border infrastructure investment, scale up flexible technologies such as long-duration storage, and promote a geographically balanced deployment of renewables to mitigate systemic risks associated with *Dunkelflaute* events.

1 INTRODUCTION

Limiting the increase in global average temperature to “well below” 2 °C requires nearly zero or even negative CO₂ emissions by mid-21st century (Rogelj et al., 2015; Davis et al., 2018). Variable renewable energy technologies such as wind power and solar photovoltaic (PV) are expected to form the foundation of future low-carbon electricity system (Schlachtberger et al., 2017; Reichenberg et al., 2018; Brown et al., 2018; Mattsson et al., 2021). As low-carbon electricity systems based on variable renewable energy (VRE) are highly weather-dependent, weather-induced uncertainties, particularly the risk of prolonged periods of low renewable output, have become a central focus of both political discussions and academic research. The term “Dunkelflaute” has become popular, even in the English language, to describe periods when the availability of wind and solar power is low, particularly the non-windy and non-sunny periods that manifest for several consecutive days (Li et al., 2020, 2021a, 2021b; Mayer et al., 2023).

It is crucial that future energy systems are designed to withstand such fluctuations in renewable resource availability. The development of mathematical optimization programs for energy system planning introduces various methodological approaches to address this challenge. Historically, most approaches exploring optimal energy systems were deterministic, based on expected or “typical” weather years. To ensure a certain level of resilience, such an optimization can be also based on a typical “worst-case” weather year. Alternatively, sampling over several historical weather years offers heuristic approaches to achieve resilience, such as averaging over the samples or imposing upper and lower bounds on generation capacities (Caglayan et al., 2021; Gøtske et al., 2024). However, a drawback is that deterministic optimization can analyze uncertainty in a post processing step only, based on exogenous parameter changes. This omits key trade-offs in decision-making, such as the coupling between proactive investments made in anticipation of uncertainty and reactive measures taken once uncertainties materialize. Furthermore, a key difficulty not addressed in these approaches, is that weather events causing extended periods of renewable scarcity, so called *Dunkelflaute*, vary across Europe in their frequency, intensity, and timing, and often affect countries unevenly. In the following we refer to the term “renewable scarcity periods” as periods of low electricity production potential from wind and/ or solar generation resources. In addition, we use the term “Dunkelflaute” to refer to a period of low electricity production potential from wind and solar resources occurring simultaneously within the same geographical zone. The impacts of such Dunkelflaute can ripple across borders, disrupt electricity flows and threatening system stability well beyond the regions directly affected.

Advances in hardware and software have allowed an expanding area of energy-system planning research to model stochasticity endogenously. The most relevant optimization technique in the context of our work is robust optimization, which seeks to find the solution that is optimal to the worst possible realization of uncertainties (i.e., worst possible scenario). While the classical robust optimization approach offers advantages in terms of computational tractability and reduced problem complexity, this comes at the expense of solution conservatism. In the context of weather uncertainty, this means that the system is designed to withstand a rare extreme event, which may never actually occur. Furthermore, classical robust optimization does not include recourse actions - adaptive responses after uncertainty is realized - limiting its ability to model operational flexibility. As a result, the solution may lead to over-investment and suboptimal performance under other weather conditions, raising concerns about economic efficiency. Adaptive robust optimization, an extension of robust optimization, improves robust optimization in that regard. It is particularly well-suited for energy systems exposed to weather-driven uncertainty, as it enables long term planning to incorporate a wide range of uncertainty realizations. This is because the adaptive robust optimization methodology consists of sequential decision-making, enabling model decisions to be adapted as the situation evolves. In this context, adaptive robust optimization iteratively identifies the worst-case weather realizations and optimizes the system accordingly.

To the best of our knowledge, our work is the first that endogenously incorporates worst-case renewable scarcity events into a European electricity system model using the adaptive robust optimization method. Compared to existing studies, our planning model derives an uncertainty range from historical weather data rather than modelling historical years. This has the advantage to compute multiple regional extreme scenarios within a single optimization run and to trace back the origin of individual worst-case scenarios. This allows us to understand their impact on the model adaptation decisions that ultimately result in a weather-robust capacity mix. Furthermore, our work advances the literature by incorporating a regional perspective into the analysis of capacity adaptation mechanisms, allowing us to identify how the burdens of adaptations are distributed within Europe.

We apply this theoretical framework to design a decarbonized electricity system for Europe in 2050 that is robust against periods of extremely low wind and solar availability. We model a whole year and represent low wind and solar availability through geographically defined events across six distinct weather zones in Europe, during a four-week period in January. This enables the model to endogenously determine where and when worst-case renewable scarcity events occur, and proactively prepares for them. As a result, the model can also account for Dunkelflaute. The research in this manuscript can be summarized as follows:

1. Develop a methodology for designing a robust European electricity system that endogenously accounts for regional renewable worst-case renewable scarcity periods such as Dunkelflaute.
2. Identify the region-specific worst-case events across Europe and quantify on both regional and system-wide costs and infrastructure requirements, providing insights into spatial vulnerabilities and adaptation needs in a fully decarbonized power system.

Our study advances the discussion on energy system robustness by deriving a single optimal solution for a European power system that is resilient to multiple endogenously generated weather uncertainty scenarios. Furthermore, we shed light on the system's adaptation mechanisms - that is, the interplay between different power technology expansion options that enhance robustness against a range of severe extreme renewable scarcity events. Compared to existing studies in the field, we investigate in detail how individual scarcity events are driving the system adaptation. Consequently, this work is interesting for the energy system modelling community and real-world energy system planners.

Section 2 reviews existing literature on weather-related events and methodological approaches to incorporate the resulting uncertainty into energy system planning. We focus particularly on optimization frameworks and empirical energy system models, thereby revealing the remaining research gap. In section 3, we introduce the underlying ARO model. Our case study is presented in section 4, and the results are discussed in section 5. We finish the paper with conclusions and a summary of the key takeaways in section 6.

2 LITERATURE REVIEW

Long-term energy system planning with a focus on extreme weather events has become increasingly popular over the last two decades. The majority¹ of papers explore weather events which impact supply and demand. Examples are heatwaves and cold periods, hydro droughts, and low solar and wind availability periods. All these topics have become relevant for electricity system planning. Low-output periods of intermittent renewables are receiving increasing attention both within academia and more broadly². For the European energy system, the impact of reduced RES availability is of major interest since a 100% renewable European system in 2050 will heavily rely on wind and solar generation technologies. Therefore, several academic studies investigate such weather events and their impacts, as well as the requirements on the current and future electricity systems to guarantee a reliable energy supply.

These investigations can be distinguished as (1) meteorological approaches, describing historical extreme weather events (e.g. Ohlendorf and Schill, 2020; Li et al., 2020, 2021a, 2021b; Jurasz et al., 2021), (2) theoretical optimization approaches, focusing on weather-related uncertainties in the planning of test systems (e.g. Jabr, 2013; Roldán et al., 2018; Roldán et al., 2019; Roldán et al., 2020), (3) approaches that utilize meteorological weather data computing renewable energy production and electricity demand to characterize critical weather events in Europe (Raynaud et al., 2018; Hannah C. Bloomfield et al., 2020; H. C. Bloomfield et al., 2020; Otero et al., 2022a; Ruhnau and Qvist, 2022; Grochowicz et al., 2024; Beck-Bang et al., 2026) and (4) empirical energy system planning models that incorporate meteorological data to address weather related uncertainty (Perera et al., 2020; Ruhnau and Qvist, 2022; Plaga and Bertsch, 2022; Grochowicz et al., 2023, 2024; Gøtske et al., 2024). As our study focusses on modelling extreme weather events within an energy system optimization framework, we place particular emphasis on reviewing the latter three categories.

Our review begins with category (2), which covers studies that address theoretical optimization approaches. In 2013, Jabr designed a robust optimization model to include the uncertainty from renewable generation and electricity load in the transmission network expansion planning process using a cardinality-constrained uncertainty set. The developed bi-level optimization problem was iteratively solved using Bender's decomposition approach (an iterative technique for mathematical programming). Testing and comparing the proposed model on various test grid systems showed that the method consistently generated reliable and cost-effective expansion plans. In a series of follow-up papers, Roldán et al., (2018, 2019, 2020), present robust model formulations, to tackle the incorporation of weather uncertainties into the transmission and generation expansion planning problem. A three-level adaptive robust optimization program was introduced to include uncertainty from wind turbines in a dynamic investment (Roldán et al., 2018). To address the disregarded correlation of uncertainty sources such as wind speed, Roldán et al. (2019) turn from using cardinal and polyhedral sets towards so-called ellipsoidal uncertainty sets.

¹ A smaller part explores how extreme events such as floods and (ice) storms impair energy infrastructure.

² Some examples: Quartz: <https://qz.com/can-europe-survive-the-dreaded-dunkelflaute-1849886529/>, a children's book named "Dunkelflaute: A Story of Renewable Wind Power" by Stephanie O'Connor (2022), Madra Rua Publishing, Donegal, Ireland, Reuters: <https://www.reuters.com/markets/commodities/german-wind-reliant-power-firms-brace-annual-dunkelflaute-2024-02-21/>

The newly developed two-stage adaptive robust optimization approach was developed further by Roldán et al. (2020) to consider the complete probability structure of uncertainty parameters, ensuring that the optimal solution found is valid. Baringo et al. (2020) developed an adaptive robust optimization model to address the expansion planning of a distribution system that incorporates solar powered electric vehicles and energy storage systems. The model considers both short-term variabilities, such as daily demand patterns, renewable variation, and long-term uncertainty, such as future peak demand and the penetration of electric vehicles. The adaptive robust optimization methodology proves to be an effective tool for distribution expansion planning by highlighting that incorporating long-term uncertainty significantly influences investment decisions. However, all these studies are conducted on test grid systems as the focus is on validating the efficiency of the optimization approaches. Consequently, the transfer of implications on real-world energy systems is limited.

Given our focus on worst-case weather events that limit wind and solar availability, we briefly review European case studies added as category (3), which analyze the effects of extreme events on renewable generation and electricity demand. In order to incorporate weather-related uncertainty in real-world energy system planning, a huge collection of existing papers uses different solution approaches and case studies. An overview is provided by, for example, Yue et al. (2018) and Conejo and Wu (2022), in which the latter points towards robust optimization methodologies used for power system planning. Raynaud et al. (2018) researched variations of so-called energy supply and production droughts across Europe and found that the individual drought, which the countries under study experience, ranged from one to seven days. While wind droughts occur more often and are present for a short period of up to three days on average for most countries, solar drought follows more of a geographical and seasonal pattern, leading to Nordic countries being more exposed to longer lasting energy drought events. Wiel et al. (2019) examined the role of weather regimes in explaining daily variations in solar PV, wind output, and electricity demand. They show that a certain day-to-day variability can be explained by identified weather regimes, which can be detected and forecasted providing valuable information for the system operating. However, the authors also state that rare extreme events cannot be precisely predicted. Bloomfield et al. (2020) studied how solar and wind generation align with demand during system stress events. They concluded that the potential of renewables to reduce residual load is limited during such scarcity conditions, and interconnectivity offers only marginal relief during high-demand and low-availability periods. Otero et al. (2022a) focused on compound periods of low wind and solar generation coinciding with high demand. They showed that such events often affect multiple European countries simultaneously, underlining the systemic risk posed by these conditions. While such studies provide valuable insights into the characteristics of extreme weather events and their impact on electricity production and demand, their relevance for energy system planning is limited due to simplified modeling approaches. Specifically, they omit critical system components such as electricity grids and storage technologies and restrict generation technologies to solar PV, wind, and run-of-river power. As their primary objective is to characterize weather phenomena rather than to inform infrastructure planning, they offer limited guidance on how future energy systems could adapt to such conditions.

These aspects are addressed in empirical studies which integrate weather-related uncertainty into energy system planning models (4). We will review that part of the literature - particularly in the European context - in the following sections to identify and synthesize the existing research gap. Perera et al. (2020) developed a hybrid stochastic-robust optimization method to investigate the impact of extreme weather events using 13 climate change scenarios on 30 cities in Sweden. They state that future climatic fluctuations and uncertainties in renewable energy potential must be incorporated into the energy system planning using suitable methods to incorporate this uncertainty endogenously. Failing to do so could hinder the integration of renewable energy into future systems and compromise the reliability of energy supply. However, the focus on Swedish cities limits the broader applicability of the findings to the European system.

In 2021, Caglayan et al. proposed a methodology to design a 100% renewable European energy system, including hydrogen infrastructure with the aim of ensuring resilience across 38 historical weather years. Their approach relies on a sequential deterministic optimization framework, and their results indicate that incorporating multiple weather years can increase system costs by approximately 25%. However, the robust system layout is restricted by several heuristic simplifications. Notably, the capacity layout for all technologies except biomass is determined based on 30 typical days from a single weather year. This limits the model's capability to incorporate rare extreme events, which are decisive for robust planning in renewable dominated systems. In a subsequent step, the model is run at hourly resolution with these capacities fixed, leaving biomass as the only technology allowed to adjust freely. This overestimates the role of biomass and underestimates the role of other flexible assets, such as long-term hydrogen, resulting in suboptimal solutions.

By employing a deterministic multi-year energy system optimization model, Ruhnau and Qvist (2022) investigated low renewable availability events within the context of a German market that would be fully powered by renewable energy systems in 2050. They analyze a period of 35 historical years, highlighting that periods of low renewable availability can continue for up to two weeks duration. They also point out that the biggest energy shortfall can cover a substantially longer period of up to nine weeks. The authors argue that focusing on short duration renewable scarcity periods or single years may result in underestimating both the storage requirements and costs of a system supplied solely by renewable sources. A limitation of the

study is its focus on Germany, which is modeled deterministically as a copper plate with fixed cross-border electricity flows, thereby neglecting the broader European system perspective.

Plaga and Bertsch (2022) apply a deterministic optimization approach to European electricity system planning under climate uncertainty. They analyze six climate scenarios from the EURO-CORDEX database individually and compare them to configurations in which multiple scenarios are modeled sequentially within a single optimization run. The results show that the system cost varies between the cheapest and most expensive scenarios by around 24 percent. Furthermore, the results show that more generation and battery storage capacity increases resilience. While their analysis focuses on the European energy system, the study is limited by analyzing only six different weather scenarios. Furthermore, a robust optimization approach that endogenously accounts for uncertainty realizations was done in this analysis.

Grochowicz et al. (2023) employed a near-optimal space method to generate a resilient European power system. Their geometric concept involves mapping the individual near-optimal feasible spaces from single deterministic weather-year optimizations, and selecting a single solution at the geometric center, providing a certain tolerance towards infeasibility across all considered periods. They found that robust layouts tend to invest more in onshore wind and solar power, leading to a 50% CO₂ emissions reduction compared to a cost optimal solution. As the method is based on intersecting multiple near-optimal solution spaces to identify cost-effective additional investments that enhance system robustness across various weather realizations, no robust optimization approach is applied. Consequently, no endogenous weather uncertainty realizations were modelled.

Also focusing on the European electricity system, Grochowicz et al. (2024) investigated “system defining events”- defined as periods that significantly impact electricity system costs - across a 41-year timespan. In addition to meteorological analysis, they employed a deterministic energy system model using nodal shadow prices and load shedding as indicators of system stress. The single year optimizations indicate that most events occur between November and February with an average duration of 7 days. However, as the focus of the study is to identify factors that characterize difficult weather events such as low temperatures, low wind, transmission congestion and storage constraints, no robust planning model was applied to incorporate weather uncertainty.

Gøtske et al. (2024) assess the impact of 62 historical weather years on a future sector-coupled, decarbonized European energy system using the PyPSA-Eur model. They conduct individual capacity optimizations for each weather year and then test the robustness of the resulting layouts by performing dispatch optimizations across all other years. Their findings highlight that low wind availability during winter poses the greatest challenge to system stability. However, since the study relies on a deterministic modeling approach, the robust system layout is effectively tailored to a single worst-case weather year. This limits the analysis’ ability to evaluate trade-offs between capacity expansion and the broader spectrum of possible weather events not captured by that specific year.

Based on this review, we can conclude the following gaps in the literature:

1. Existing theoretical studies apply robust optimization approaches on test systems, offering valuable theoretical insights but limited empirical contributions.
2. Empirical energy system planning studies rely on deterministic and heuristic optimization approaches rather than robust optimization to incorporate weather-related uncertainty.
3. Existing energy system planning studies focus their analysis primarily on the overall system design, omitting deeper insights into how renewable scarcity events impact regional electricity supply and adaptation strategies.

While the reviewed contributions offer valuable insights, most studies focus on analyzing the effect of extreme events at system level. Furthermore, the exogenous treatment of uncertain renewable availability periods based on historical weather realizations limits the investigation space of future system adaptation needs to specific recorded events. In contrast, our robust optimization approach just controls the geographical scope and time dimension of extreme scarcity events. The model itself pinpoints which conditions constitute worst-case scarcity events and where they originate. This enables us to trace the origin of individual worst-case scenarios and analyze their impact on model results. This allows us to identify the events that drive system adaptation and associated costs. Furthermore, we complement the insights into the adaptation process with an analysis down to a regional (country) level in the modelled system. Therefore, we developed an adaptive robust optimization framework (ARO) that integrates regionally differentiated wind and/or solar scarcity periods into a detailed planning model for a decarbonized European power system in 2050. Despite its strong theoretical foundation, robust optimization has not yet been applied to address weather-related uncertainty in long-term electricity system planning at a European scale. In doing so, we also demonstrate both the practical applicability and the added value of robust optimization approaches for real-world energy system design under deep uncertainty.

3 METHODOLOGY

In this study, we formulate a long-term generation and transmission expansion planning problem from a central planner's perspective. The energy system model optimizes investment decisions under uncertainty using the ARO method. The process is explained in more detail in Appendix A. In short, a Master Problem (I) and the Subproblem (II) are established, which can be iteratively solved using the column and constraint generation algorithm. During this process, the Master Problem transfers information on expansion of infrastructure assets such as generation, storage, and transmission in set $\Phi^{M \rightarrow S}$ to the Subproblem, which sends back information about worst case realizations and corrective actions in set $\Phi^{S \rightarrow M}$ to the Master Problem. This process continues until the objective values of both problems converge to a previously defined value. The interested reader is referred to the book by Conejo et al. (2016), which details an extensive explanation of the column and constraint generation algorithm.

3.1 Expansion decisions (Master problem)

Nomenclature	
Indices	
t	Time steps
n	Nodes
l	Transmission lines, AC and DC
r	Solar & wind generation units
c	Conventional (conv.) generation units
b	Battery storage unit
h	Hydrogen storage unit
ror	Hydro run of river plant
rsv	Hydro reservoir plant
psp	Hydro pumping storage plant
g	Geographical weather region
Sets	
$r(l)$	Receiving node of transmission line
$s(l)$	Sending node of transmission line
$AC(l)$	Alternating current Transmission line
$DC(l)$	Direct current Transmission line
Φ^D	Primal variables in Master Problem
Φ^U	Uncertainty set
Φ^S	Dual variables in Subproblem
Φ_n^R	Solar, wind power plants located at node n
Φ_n^P	Conventional power plants located at node n
Φ_n^B	Battery storage units located at node n
Φ_n^H	Hydrogen storage units located at node n
Φ_n^{ROR}	Run of river plants located at node n
Φ_n^{PSP}	Pumping storage plants located at node n
Φ_n^{RSV}	Hydro reservoir plant located at node n
$pv(r)$	Solar PV power plants
$wind(r)$	Wind turbines
$ref(n)$	Slack or reference node
Scalars	
f^{L1}	Percentage of flexible demand level 1
f^{L2}	Percentage of flexible demand level 2
f^{L3}	Percentage of flexible demand level 3
M	Large scalar value
Γ_r	Uncertainty budget for renewable unit
Parameters	
$dem_{n,t}$	Electricity demand at node and time step [MWh]
ac_r	Annualized investments costs for solar & wind generation units [EUR/MW]
ac_b^{INV}	Annualized investments costs for battery inverter of battery storage units [EUR/MW]
\overline{cap}_{rsv}	Existing rsv generation capacity [MW]
\overline{cap}_{psp}	Existing psp generation capacity [MW]
\overline{cap}_l	Existing transmission line capacity [MW]
$\overline{cf}_{r,t}$	Expected solar & wind capacity factors
$\widehat{cf}_{r,t}$	Solar, wind capacity factors maximum deviation
$\overline{cf}_{r,t}^M$	Solar, wind capacity factors realization
csf_{psp}	Capacity scaling factor for pumping storage plants
$af_{rsv,t}$	Hydro reservoir availability factor
σ_{psp}	Efficiency of pumping storage plant
σ_b	Efficiency of battery inverter
σ_h^{EL}	Efficiency of electrolyzer
σ_h^{OCGT}	Efficiency of H ₂ -fired open cycle gas turbine
\overline{sub}_r^{REN}	Solar, wind capacity in subproblem [MW]
\overline{sub}_b^{INV}	Capacity of battery inverter in subproblem [MW]
\overline{sub}_b^{STOR}	Battery storage capacity in subproblem [MWh]
\overline{sub}_h^{OCGT}	Capacity of H ₂ -fired OCGT in subproblem [MW]
\overline{sub}_h^{EL}	Capacity of electrolyzer in subproblem [MW]
\overline{sub}_h^{STOR}	Hydrogen storage capacity in subproblem [MWh]
\overline{sub}_l^{line}	Transmission line capacity in subproblem [MW]
Positive Variables	
CAP_r	Capacity of solar, wind generation unit [MW]
CAP_b^{INV}	Capacity of battery inverter unit [MW]
CAP_b^{STOR}	Storage capacity of battery unit [MWh]
CAP_h^{OCGT}	Capacity of H ₂ -fired OCGT unit [MW]
CAP_h^{EL}	Capacity of electrolyzer unit [MW]
CAP_h^{STOR}	Storage capacity of hydrogen storage unit [MWh]
CAP_l	Transmission line capacity [MW]
$GEN_{c,t}$	Generation of conv. unit [MWh]
$GEN_{r,t}$	Generation of solar & wind unit [MWh]
$GEN_{ror,t}$	Generation of ror. unit [MWh]
$GEN_{rsv,t}$	Generation of rsv. unit [MWh]
$GEN_{psp,t}$	Generation of psp unit [MWh]
$CH_{psp,t}$	Charging of psp. unit [MWh]
$CH_{h,t}$	Charging of hydrogen storage [MWh]
$CH_{b,t}$	Charging of battery unit [MWh]
$LVL_{psp,t}$	Storage filling level of psp. unit [MWh]
$LVL_{b,t}$	Storage filling level of battery storage [MWh]
$LVL_{h,t}$	Storage filling level of hydrogen storage [MWh]
$LS_{n,t}^{L1}$	Load shedding level 1 [MWh]
$LS_{n,t}^{L2}$	Load shedding level 2 [MWh]
$LS_{n,t}^{L3}$	Load shedding level 3 [MWh]

ac_b^{STOR}	Annualized investments costs for battery storage units [EUR/MWh]	$\overline{Cf}_{r,t}$	Uncertain renewable capacity factor
ac_h^{OCGT}	Annualized investments costs for H ₂ -fired open cycle gas turbine [EUR/MW]	$PF_{l,t}$	Line power flow [MWh]
ac_h^{EL}	Annualized investments costs for electrolyzer [EUR/MW]	$\theta_{s/r(l)}$	Voltage angle receiving/ sending line
ac_h^{STOR}	Annualized investments costs for H ₂ storage [EUR/MWh]	Binary Variables	
ac_l	Annualized investment costs for transmission line [EUR/MW]	$Z_{r,t}$	Variable representing the deviation from reference solar, wind capacity factor
vc_c	Variable costs of conv. generation [EUR/MWh]	Auxiliary Variables	
sc_n^{LS1}	Level 1 load shedding costs at node n [EUR/MW]	$\phi_{r,t}^{aux}$	Variable used for linearization
sc_n^{LS2}	Level 2 load shedding costs at node n [EUR/MW]	Dual Variables	
sc_n^{LS3}	Level 3 load shedding costs at node n [EUR/MW]	(·)	Dual variables are provided after the corresponding equalities or inequalities separated by a colon
\overline{cap}_c	Existing conv. generation capacity [MW]		
\overline{cap}_{ror}	Existing ror generation capacity [MW]		

The first problem, the Master Problem, is a deterministic linear optimization program utilizing the DC optimal power flow method to minimize the investment and generation costs. A detailed model formulation is provided in the following with the optimization variables are denoted in the set $\Phi^D = \{ CAP_{pv}; CAP_{wind}; CAP_b^{INV}; CAP_b^{STOR}; CAP_h^{OCGT}; CAP_h^{EL}; CAP_h^{STOR}; CAP_l; GEN_{c,t}; GEN_{r,t}; GEN_{ror,t}; GEN_{rsv,t}; GEN_{psp,t}; CH_{psp,t}; CH_{h,t}; CH_{b,t}; LVL_{psp,t}; LVL_{b,t}; LVL_{h,t}; PF_{l,t}; S_{n,t}^{LS1}; S_{n,t}^{LS2}; S_{n,t}^{LS3}; \theta_{s/r(l)} \}$:

$$\begin{aligned}
\text{Min}_{\Phi^D} : & \sum_{pv} CAP_{pv} \cdot ac_{pv} + \sum_{wind} CAP_{wind} \cdot ac_{wind} \\
& + \sum_b CAP_b^{INV} \cdot ac_b^{INV} + \sum_b CAP_b^{STOR} \cdot ac_b^{STOR} + \sum_h CAP_h^{OCGT} \cdot ac_h^{OCGT} + \sum_h CAP_h^{EL} \cdot ac_h^{EL} \\
& + \sum_h CAP_h^{STOR} \cdot ac_h^{STOR} + \sum_l CAP_l \cdot ac_l + \sum_{c,t} GEN_{c,t} \cdot vc_c + \sum_{n,t} LS_{n,t}^{L1} \cdot sc_n^{LS1} \\
& + \sum_{n,t} LS_{n,t}^{L2} \cdot sc_n^{LS2} + \sum_{n,t} LS_{n,t}^{L3} \cdot sc_n^{LS3}
\end{aligned} \tag{1}$$

subject to

$$\begin{aligned}
dem_{n,t} - LS_{n,t}^{L1} - LS_{n,t}^{L2} - LS_{n,t}^{L3} \\
= \sum_{r \in \Phi_n^{pv}} GEN_{pv,t} + \sum_{r \in \Phi_n^{wind}} GEN_{wind,t} + \sum_{c \in \Phi_n^c} GEN_{c,t} + \sum_{ror \in \Phi_n^{ROR}} GEN_{ror,t} + \sum_{rsv \in \Phi_n^{RSV}} GEN_{rsv,t} \\
+ \sum_{psp \in \Phi_n^{PSP}} (GEN_{psp,t} - CH_{psp,t}) + \sum_{h \in \Phi_n^H} (GEN_{h,t} - CH_{h,t}) + \sum_{b \in \Phi_n^B} (GEN_{b,t} - CH_{b,t}) \\
+ \sum_{l \in r(l)} PF_{l,t} - \sum_{l \in s(l)} PF_{l,t} : \lambda_{n,t}, \forall n, t
\end{aligned} \tag{2}$$

$$GEN_{pv,t} \leq CAP_{pv} \cdot \overline{cf}_{pv,t}^M : \mu_{pv,t}^R, \forall pv(r), g, t \tag{3}$$

$$GEN_{wind,t} \leq CAP_{wind} \cdot \overline{cf}_{wind,t}^M : \mu_{wind,t}^R, \forall wind(r), g, t \tag{4}$$

$$GEN_{c,t} \leq \overline{cap}_c : \mu_{c,t}^{CONV}, \forall c, t \tag{5}$$

$$GEN_{ror,t} \leq \overline{cap}_{ror} : \mu_{ror,t}^{ROR}, \forall ror, t \tag{6}$$

$$GEN_{rsv,t} \leq \overline{cap}_{rsv} \cdot af_{rsv,t} : \mu_{rsv,t}^{RSV}, \forall rsv, t \tag{7}$$

$$GEN_{psp,t} \leq \overline{cap}_{psp} : \mu_{psp,t}^{DIS}, \forall psp, t \tag{8}$$

$$CH_{psp,t} \leq \overline{cap}_{psp} : \mu_{psp,t}^{CH}, \forall psp, t \tag{9}$$

$$LVL_{psp,t} \leq \overline{cap}_{psp} \cdot csf_{psp} : \mu_{psp,t}^{CAP}, \forall psp, t \tag{10}$$

$$LVL_{pssp,t=1} = \frac{(cap_{pssp} \cdot csf_{pssp})}{2} + (CH_{pssp,t=1} \cdot \sigma_{pssp}) - GEN_{pssp,t=1} : \phi_{pssp,t=1}^{LVL}, \forall pssp \quad (11)$$

$$LVL_{pssp,t} = LVL_{pssp,t-1} + (CH_{pssp,t} \cdot \sigma_{pssp}) - GEN_{pssp,t} : \phi_{pssp,t}^{LVL}, \forall pssp, \forall t > 1, \quad (12)$$

$$GEN_{b,t} \leq CAP_b^{INV} : \mu_{b,t}^{DB}, \forall b, t \quad (13)$$

$$CH_{b,t} \leq CAP_b^{INV} : \mu_{b,t}^{CB}, \forall b, t \quad (14)$$

$$LVL_{b,t} \leq CAP_b^{STOR} : \mu_{b,t}^{APB}, \forall b, t \quad (15)$$

$$LVL_{b,t=1} = (CH_{b,t=1} \cdot \sigma_b) - GEN_{b,t=1} : \phi_{b,t=1}^{LVLB}, \forall b \quad (16)$$

$$LVL_{b,t} = LVL_{b,t-1} + (CH_{b,t} \cdot \sigma_b) - GEN_{b,t} : \phi_{b,t}^{LVLB}, \forall b, \forall t > 1, \quad (17)$$

$$GEN_{h,t} \leq CAP_h^{OCGT} : \mu_{h,t}^{OCGT}, \forall h, t \quad (18)$$

$$CH_{h,t} \leq CAP_h^{EL} : \mu_{h,t}^{EL}, \forall h, t \quad (19)$$

$$LVL_{h,t} \leq CAP_h^{STOR} : \mu_{h,t}^{APH}, \forall h, t \quad (20)$$

$$LVL_{h,t=1} = (CH_{h,t=1} \cdot \sigma_h^{EL}) - \frac{GEN_{h,t=1}}{\sigma_h^{OCGT}} : \phi_{h,t=1}^{LVLH}, \forall h \quad (21)$$

$$LVL_{h,t} = LVL_{h,t-1} + (CH_{h,t} \cdot \sigma_h^{EL}) - \frac{GEN_{h,t}}{\sigma_h^{OCGT}} : \phi_{h,t}^{LVLH}, \forall h, \forall t > 1, \quad (22)$$

$$PF_{l,t} = sus_l \cdot (\theta_{s(l)} - \theta_{r(l)}) : \phi_{l,t}^L, \forall l, t \quad (23)$$

$$-(\overline{cap}_l + CAP_l) \leq PF_{l,t} \leq \overline{cap}_l + CAP_l : \underline{\mu}_{l,t}^L, \overline{\mu}_{l,t}^L, \forall l, t \quad (24)$$

$$-\pi \leq \theta_{n,t} \leq \pi : \underline{\mu}_{n,t}^N, \overline{\mu}_{n,t}^N, \forall n, t \quad (25)$$

$$\theta_{n,t} = 0 : \epsilon^{ref}, \quad n \in ref(n) \quad (26)$$

$$LS_{n,t}^{L1} \leq dem_{n,t} \cdot f^{L1} : \mu_{n,t}^{LS1}, \forall n, t \quad (27)$$

$$LS_{n,t}^{L2} \leq dem_{n,t} \cdot f^{L2} : \mu_{n,t}^{LS2}, \forall n, t \quad (28)$$

$$LS_{n,t}^{L3} \leq dem_{n,t} \cdot f^{L3} : \mu_{n,t}^{LS3}, \forall n, t \quad (29)$$

The objective function in Eq. (1) minimizes the sum of the annualized renewable capacity and transmission investment costs, the annualized costs of the battery storage systems, which includes inverter and storage cost components, the annualized costs of the hydrogen storage systems, which include the electrolyzer, the H₂ storage tank and the H₂ fired open cycle gas turbines (OCGTs) power plant, as well as the variable generation costs and the load shedding costs. The minimization problem is subject to several constraints such as the energy balance in Eq. (2), the technical generation constraints of renewable generation units, considering the capacity factors for solar PV and wind ($\overline{cf}_{pv,t}^M, \overline{cf}_{wind,t}^M$) in Eqs. (3-4), the conventional generation in Eq. (5), and hydropower generation in Eqs. (6-7), the storage constraints for pumping storage plants in Eqs. (8-12), battery storages in Eqs. (13-17) and hydrogen storage in Eqs. (18-22). The model does not consider an underlying hydrogen transmission network. Therefore, hydrogen storage tanks located at a specific node can only be charged or discharged by collocated electrolyzer and hydrogen-fired OCGT power plants that consume electricity or hydrogen, respectively.

We consider DC power flow constraints in Eqs. (23-26), and three load shedding constraints in Eqs. (27-29). Note that these three load shedding constraints establish a stepwise load shedding curve, where the factors f^{L1}, f^{L2}, f^{L3} (with $f^{L1} < f^{L2} < f^{L3}$) represent specific percentages of demand at a given node and time. The load shedding variables $LS_{n,t}^{L1}, LS_{n,t}^{L2}, LS_{n,t}^{L3}$ are multiplied with different cost levels in the objective function. This implementation creates a stepwise load shedding cost function, enabling the model to utilize varying degrees of load flexibility at different cost levels.

3.1 Worst case realizations and corrective actions (Subproblem)

Our approach to modeling uncertainty as the realization of low solar PV and wind availability involves defining cardinality-constrained uncertainty sets for these renewable generation technologies. To avoid confusion between general descriptive language and model-specific terminology in the reminder, we introduce the following distinction: the term extreme weather

event is used generically to describe scarcity periods of significantly reduced renewable generation, whether due to low wind, low solar, or both. In contrast, a worst-case renewable scarcity event refers to a specific uncertainty realization identified within our adaptive robust optimization framework, representing the most adverse combination of low renewable availability for system planning.

The cardinality-constrained uncertainty set Φ^U controls the number of uncertain parameters that can deviate from their nominal values. This is controlled by binary variables Z in combination with the uncertainty budget Γ , and can be described formally as follows:

$$\Phi^U = \left\{ \begin{array}{l} \overline{Cf}_{r,g,t} = \widetilde{c}f_{r,g,t} - \sum_{p \in P(t)} Z_{r,g,p} \cdot \widehat{c}f_{r,g,t} \quad \forall r, \forall g, \forall t, \forall p \\ Z_{r,g,p} \in \{0,1\} \quad \forall r, \forall g, \forall p \\ \sum_{g \in G} Z_{r,g,p} \leq \Gamma_{r,p} \quad \forall r, \forall p \end{array} \right\} \quad (30)$$

Equation (30) describes the uncertain renewable capacity factor variable $\overline{Cf}_{r,n,g,t}$ for a specific renewable technology r (solar PV or wind), located in weather region g and time step t depending on the reference value $\widetilde{c}f_{r,g,t}$ (expected historical average) and the deviation values $\widehat{c}f_{r,g,t}$. The realization of the deviation depends on the value of the binary variable $Z_{r,g,p}$, defined by eq. (31). Note here, that the binary variable is defined over a certain period p . The period p is defining a time horizon, spanning over several timesteps, such as a day, week, or month including several hours. The Subproblem then calculates both the most unfortunate uncertainty realizations with respect to the variables in the set Φ^U and the corrective dispatch actions of variables in set $\Phi^S = \{\mu_{c,t}^{Conv}; \mu_{pv,t}^R; \mu_{wind,t}^R; \mu_{ror,t}^{ROR}; \mu_{rsv,t}^{RSV}; \mu_{psp,t}^{DIS}; \mu_{psp,t}^{CH}; \mu_{b,t}^{CAPB}; \mu_{h,t}^{EL}; \mu_{h,t}^{OCGT}; \mu_{h,t}^{CAPH}; \mu_{n,t}^{LS1}; \mu_{n,t}^{LS2}; \mu_{n,t}^{LS3}; \underline{\mu}_{l,t}^L; \underline{\mu}_{l,t}^L; \mu_{n,t}^N; \phi_{pv,t}^{aux}; \phi_{wind,t}^{aux}; \lambda_{n,t}; \phi_{l,t}^L; \phi_{psp,t}^{LVL}; \phi_{b,t}^{LVLB}; \phi_{h,t}^{LVLH}; \epsilon^{ref}\}$, maximizing the total system cost. Set Φ^S is also referred to as feasibility set. Note that the model endogenously and solely computes the worst-case scarcity event realizations based on the impact on the total system cost. On this basis, the model can consider either scarcity events of a single renewable technology in a specific region or the simultaneous scarcity of both. If both wind and solar availability are simultaneously reduced, we refer to this as a worst-case ‘‘Dunkelflaute’’ event.

The resulting Subproblem takes the following form:

$$\begin{aligned} & \text{Max} \\ & \Phi^U \Phi^S \end{aligned} \quad (33)$$

$$\begin{aligned} & \sum_{n,t} \lambda_{n,t} \cdot dem_{n,t} + \sum_{c,t} -\mu_{c,t}^{Conv} \cdot \overline{cap}_c + \sum_{pv,t} -\mu_{pv,t}^R \cdot (\overline{sub}_{pv}^{REN} \cdot \widetilde{c}f_{pv,t}) + \phi_{pv,t}^{aux} \cdot (\overline{sub}_{pv}^{REN} \cdot \widehat{c}f_{pv,t}) \\ & + \sum_{wind,t} -\mu_{wind,t}^R \cdot (\overline{sub}_{wind}^{REN} \cdot \widetilde{c}f_{wind,t}) + \phi_{wind,t}^{aux} \cdot (\overline{sub}_{wind}^{REN} \cdot \widehat{c}f_{wind,t}) \\ & + \sum_{ror,t} -\mu_{ror,t}^{ROR} \cdot \overline{cap}_{ror} + \sum_{rsv,t} -\mu_{rsv,t}^{RSV} \cdot (\overline{cap}_{rsv} \cdot af_{rsv,t}) \\ & + \sum_{psp,t} -\mu_{psp,t}^{DIS} \cdot \overline{cap}_{psp} - \mu_{psp,t}^{CH} \cdot \overline{cap}_{psp} - \mu_{psp,t}^{CAP} \cdot (\overline{cap}_{psp} \cdot csf_{psp}) \\ & + \sum_{psp,t=1} \phi_{psp,t=1}^{LVL} \cdot \frac{\overline{cap}_{psp} \cdot csf_{psp}}{2} \\ & + \sum_{b,t} -\mu_{b,t}^{DB} \cdot \overline{sub}_b^{INV} - \mu_{b,t}^{CB} \cdot \overline{sub}_b^{INV} - \mu_{b,t}^{CAPB} \cdot \overline{sub}_b^{STOR} \\ & + \sum_{h,t} -\mu_{h,t}^{OCGT} \cdot \overline{sub}_h^{OCGT} - \mu_{h,t}^{EL} \cdot \overline{sub}_h^{EL} - \mu_{h,t}^{CAPH} \cdot \overline{sub}_h^{STOR} \\ & + \sum_{n,t} -\mu_{n,t}^{LS1} \cdot (dem_{n,t} \cdot f^{L1}) + \sum_{n,t} -\mu_{n,t}^{LS2} \cdot (dem_{n,t} \cdot f^{L2}) \\ & + \sum_{n,t} -\mu_{n,t}^{LS3} \cdot (dem_{n,t} \cdot f^{L3}) + \sum_{l,t} -\underline{\mu}_{l,t}^L \cdot \overline{sub}_l^{Line} + \sum_{l,t} -\overline{\mu}_{l,t}^L \cdot \overline{sub}_l^{Line} \end{aligned}$$

$$\overline{Cf}_{pv,g,t} = \widetilde{c}f_{pv,g,t} - \sum_{p \in P(t)} Z_{pv,g,p} \cdot \widehat{c}f_{pv,g,t} \quad \forall pv(r), \forall g, \forall t, \forall p \quad (34)$$

$$\overline{cf}_{wind,g,t} = \widetilde{cf}_{wind,g,t} - \sum_{p \in P(t)} Z_{wind,g,p} \cdot \widehat{cf}_{wind,g,t} \quad \forall wind(r), \forall g, \forall t, \forall p \quad (35)$$

$$\sum_{g \in G} Z_{pv,g,p} \leq \Gamma_{pv,p} \quad \forall pv(r), \forall p \quad (36)$$

$$\sum_{g \in G} Z_{wind,g,p} \leq \Gamma_{wind,p} \quad \forall wind(r), \forall p \quad (37)$$

$$\lambda_{n,t} - \mu_{c,t}^{Conv} \leq 0, \quad \forall n, \forall c, \forall t \quad (38)$$

$$\lambda_{n,t} - \mu_{pv,t}^R \leq 0, \quad \forall n, \forall pv(r), \forall t \quad (39)$$

$$\lambda_{n,t} - \mu_{wind,t}^R \leq 0, \quad \forall n, \forall wind(r), \forall t \quad (40)$$

$$\lambda_{n,t} - \mu_{ror,t}^{ROR} \leq 0, \quad \forall n, \forall ror, \forall t \quad (41)$$

$$\lambda_{n,t} - \mu_{rsv,t}^{RSV} \leq 0, \quad \forall n, \forall rsv, \forall t \quad (42)$$

$$\lambda_{n,t} - \phi_{PSP,t}^{LVL} - \mu_{PSP,t}^{DIS} \leq 0, \quad \forall n, \forall psp, \forall t \quad (43)$$

$$-\lambda_{n,t} + \phi_{PSP,t}^{LVL} \cdot \sigma_{psp} - \mu_{psp,t}^{CH} \leq 0, \quad \forall n, \forall psp, \forall t \quad (44)$$

$$\phi_{PSP,t}^{LVL} - \phi_{PSP,t-1}^{LVL} - \mu_{PSP,t}^{CAP} + \underline{\mu}_{PSP,t}^{CAP} = 0, \quad \forall psp, \forall t \quad (45)$$

$$\phi_{PSP,t=1}^{LVL} - \mu_{PSP,t=1}^{CAP} + \underline{\mu}_{PSP,t=1}^{CAP} = 0, \quad \forall psp \quad (46)$$

$$\lambda_{n,t} - \phi_{b,t}^{LVLB} - \mu_{b,t}^{DB} \leq 0, \quad \forall n, \forall b, \forall t \quad (47)$$

$$-\lambda_{n,t} + \phi_{b,t}^{LVLB} \cdot \sigma_b - \mu_{b,t}^{CB} \leq 0, \quad \forall n, \forall b, \forall t \quad (48)$$

$$-\phi_{b,t}^{LVLB} + \phi_{b,t+1}^{LVLB} - \mu_{b,t}^{CAPB} + \underline{\mu}_{b,t}^{CAPB} = 0, \quad \forall b, \forall t \in T \setminus \{t_{last}\} \quad (49)$$

$$-\phi_{b,t}^{LVLB} - \mu_{b,t}^{CAPB} + \underline{\mu}_{b,t}^{CAPB} = 0, \quad \forall b, \forall t_{last} \quad (50)$$

$$\lambda_{n,t} - \frac{\phi_{h,t}^{LVLH}}{\sigma_h^{OCGT}} - \mu_{h,t}^{OCGT} \leq 0, \quad \forall n, \forall h, \forall t \quad (51)$$

$$-\lambda_{n,t} + \phi_{h,t}^{LVLH} \cdot \sigma_h^{EL} - \mu_{h,t}^{EL} \leq 0, \quad \forall n, \forall h, \forall t \quad (52)$$

$$-\phi_{h,t}^{LVLH} + \phi_{h,t+1}^{LVLH} - \mu_{h,t}^{CAPH} + \underline{\mu}_{h,t}^{CAPH} = 0, \quad \forall h, \forall t \in T \setminus \{t_{last}\} \quad (53)$$

$$-\phi_{h,t}^{LVLH} - \mu_{h,t}^{CAPH} + \underline{\mu}_{h,t}^{CAPH} = 0, \quad \forall h, \forall t_{last} \quad (54)$$

$$\lambda_{n,t} - \mu_{n,t}^{LS1} \leq sc_n^{LS1}, \quad \forall n, \forall t \quad (55)$$

$$\lambda_{n,t} - \mu_{n,t}^{LS2} \leq sc_n^{LS2}, \quad \forall n, \forall t \quad (56)$$

$$\lambda_{n,t} - \mu_{n,t}^{LS3} \leq sc_n^{LS3}, \quad \forall n, \forall t \quad (57)$$

$$-\lambda_{s(l)} + \lambda_{r(l)} - \overline{\mu}_{l,t}^L + \underline{\mu}_{l,t}^L + \phi_{l,t}^L = 0, \quad \forall t, \forall l \in AC(l) \quad (58)$$

$$-\lambda_{s(l)} + \lambda_{r(l)} - \overline{\mu}_{l,t}^L + \underline{\mu}_{l,t}^L = 0, \quad \forall t, \forall l \in DC(l) \quad (59)$$

$$\sum_{s(l)} (sus_l \cdot \phi_{l,t}^L) - \sum_{r(l)} (sus_l \cdot \phi_{l,t}^L) - \underline{\mu}_{n,t}^N + \overline{\mu}_{n,t}^N = 0, \quad \forall n, \forall t \quad (60)$$

$$\sum_{s(l)} (sus_l \cdot \phi_{l,t}^L) - \sum_{r(l)} (sus_l \cdot \phi_{l,t}^L) - \underline{\mu}_{n,t}^N + \overline{\mu}_{n,t}^N + \epsilon^{ref} = 0, \quad \forall n, \forall t \quad (61)$$

$$(-M) \cdot Z_{pv,g,p} \leq \phi_{pv,t}^{aux} \leq M \cdot Z_{pv,g,p}, \quad \forall pv(r), \forall g, \forall p, \forall t \quad (62)$$

$$(-M) \cdot (1 - Z_{pv,g,p}) \leq \mu_{pv,t}^R - \phi_{pv,t}^{aux} \leq M \cdot (1 - Z_{pv,g,p}), \quad \forall pv(r), \forall g, \forall p, \forall t \quad (63)$$

$$(-M) \cdot Z_{wind,g,p} \leq \phi_{wind,t}^{aux} \leq M \cdot Z_{wind,g,p}, \quad \forall wind(r), \forall g, \forall p, \forall t \quad (64)$$

$$(-M) \cdot (1 - Z_{wind,g,p}) \leq \mu_{wind,t}^R - \phi_{wind,t}^{aux} \leq M \cdot (1 - Z_{wind,g,p}), \quad \forall wind(r), \forall g, \forall p, \forall t \quad (65)$$

$$\text{Positive variables: } \mu_{c,t}^{Conv}; \mu_{pv,t}^R; \mu_{wind,t}^R; \mu_{ror,t}^R; \mu_{rsv,t}^R; \mu_{psp,t}^{DIS}; \mu_{psp,t}^{CH}; \mu_{b,t}^{CAPB}; \mu_{h,t}^{EL}; \mu_{h,t}^{OCGT}; \mu_{h,t}^{CAPH}; \quad (66)$$

$$\mu_{n,t}^{LS1}; \mu_{n,t}^{LS2}; \mu_{n,t}^{LS3}; \bar{\mu}_{l,t}^L; \underline{\mu}_{l,t}^L; \bar{\mu}_{n,t}^N; \underline{\mu}_{n,t}^N; \phi_{pv,t}^{aux}; \phi_{wind,t}^{aux}$$

$$\text{Free variables: } \lambda_{n,t}; \phi_{l,t}^L; \phi_{psp,t}^{LVL}; \phi_{b,t}^{LVLB}; \phi_{h,t}^{LVLH}; \epsilon^{ref} \quad (67)$$

Note that within the formulation of the Master Problem, the renewable availability constraints (3) and (4) are determined as variables by the Subproblem which maximizes the objective function by identifying the most unfortunate realization of $\bar{Cf}_{wind,g,t}$ and $\bar{Cf}_{wind,g,t}$, defined by Eqs. (34)-(37). The dual generation constraints of the conventional generators, the renewable generators, and the hydro generators are described by Eqs. (38)-(42). The dual storage reformulation for the pumped hydro storage is defined by Eqs. (43-46), followed by the dual battery storage formulation in Eqs. (47)-(50), and by the dual hydrogen storage formulation from Eqs. (51)-(54). The dual load shedding formulation is described by Eqs. (55)-(57), followed by the dual formulation of the transmission line flows in Eqs. (58)-(61). We use the big M constraints in Eqs. (62)-(65) and introduce the auxiliary variables $\phi_{pv,t}^{aux}$ and $\phi_{wind,t}^{aux}$ to replace the non-linear term in the objective function $\mu_{pv,t}^R \cdot \bar{Cf}_{pv,g,t}$ and $\mu_{wind,t}^R \cdot \bar{Cf}_{wind,g,t}$ with an equivalent linear formulation. The dual variable types are declared in Eqs. (66) and (67).

The problem is solved with a column-constraint generation algorithm that iterates over the Master Problem and Subproblems until a predefined convergence tolerance between the two objective functions is archived. Therefore, information between the Master and the Subproblem is exchanged, as visualized in Figure 8. From the Master Problem, the generation and transmission capacity expansion decisions are transferred to the Subproblem by storing the information in the following parameter set $\Phi^{M \rightarrow S} = \{\bar{sub}_{pv}^{REN}; \bar{sub}_{wind}^{REN}; \bar{sub}_b^{INV}; \bar{sub}_b^{STOR}; \bar{sub}_h^{OCGT}; \bar{sub}_h^{EL}; \bar{sub}_h^{STOR}; \bar{sub}_l^{Line}\}$. The Subproblem stores the information of the renewable capacity factors worst case realizations in parameters $\bar{cf}_{pv,t}^M$ and $\bar{cf}_{wind,t}^M$, and sends the information to the Master Problem, described by set $\Phi^{S \rightarrow M} = \{\bar{Cf}_{pv,g,t} \rightarrow \bar{cf}_{pv,t}^M; \bar{Cf}_{wind,g,t} \rightarrow \bar{cf}_{wind,t}^M\}$.

4 APPLICATION – CASE STUDY

For our study we develop a generation and transmission expansion planning model for a 100% renewable electricity system for 24 European countries with the planning horizon of 2050. We use PyPSA-Eur to cluster the ENTSO-E transmission system data to generate the underlying electricity system with 50 nodes and 97 transmission lines and links as depicted in Figure 1. The model differentiates expandable and non-expandable generation technologies. Expandable generation technologies allow endogenous investment in new capacity comprising solar PV, onshore wind, offshore wind (where coastal connections exist), hydrogen storage, electrolyzers, hydrogen-fired open cycle gas turbines (OCGT), battery storage, and inverters. Also, the transmission line capacity can be expanded. However, expansion is limited to an additional 100 % of 2020 levels (i.e. ENTSO-E's TYNDP 2024 assumes up to 75 % by 2040). Non-endogenous capacities comprise hydro and nuclear power. We fix hydro power, which includes run-of-river (RoR), reservoir and pumping storage power plants, at their current levels since we assume that expansion potential is negligible. For nuclear power capacity in 2050, we consider existing power plants that will still be in operation in 2050, given a lifetime of 60 years, as well as newly planned nuclear power projects based on data from the World Nuclear Association. Details on the specific technology data and costs are presented in Appendix B.

The electricity demand for each node in 2050 was estimated using the open-source GlobalEnergyGIS package based on Mattsson et al. (2021). First, we projected annual electricity consumption for each region in 2050 based on 2016 demand data taken from the International Energy Agency, and regional growth in the Shared Socioeconomic Pathway 2 scenario from Riahi et al. (2017). Then, we estimated the hourly demand profile using a machine learning model that applies historical demand data from 44 countries to a gradient boosting regression approach based on Friedman (2001). This model incorporates calendar effects (e.g. hour of day, weekday/weekend), temperature (e.g. hourly temperature in key population areas), and economic indicators (e.g. local gross domestic product per capita). Finally, the hourly demand series is scaled to match the projected annual demand for each region in 2050.

To incorporate weather data, we analyzed 40 historical weather years based on data from the Renewable.ninja website (data are based on the works of Pfenninger and Staffell (2016), and Staffell and Pfenninger (2016)). For each node in the system, we include individual historical average capacity factor time series for solar PV, and onshore and offshore wind technologies. To enhance the model's tractability, we apply a time series reduction method (moving average) on the demand and renewable capacity factor time series. Consequently, our model includes an entire year with 4-hour timesteps. In the following section,

we describe the parameterization of the weather-related uncertainty and present the scenarios of the case study that determine the geographical coverage of the wind and solar scarcity events. To support transparency and reproducibility, all data, code, and results are publicly available on GitHub³, allowing readers to verify, adapt, or extend our work.

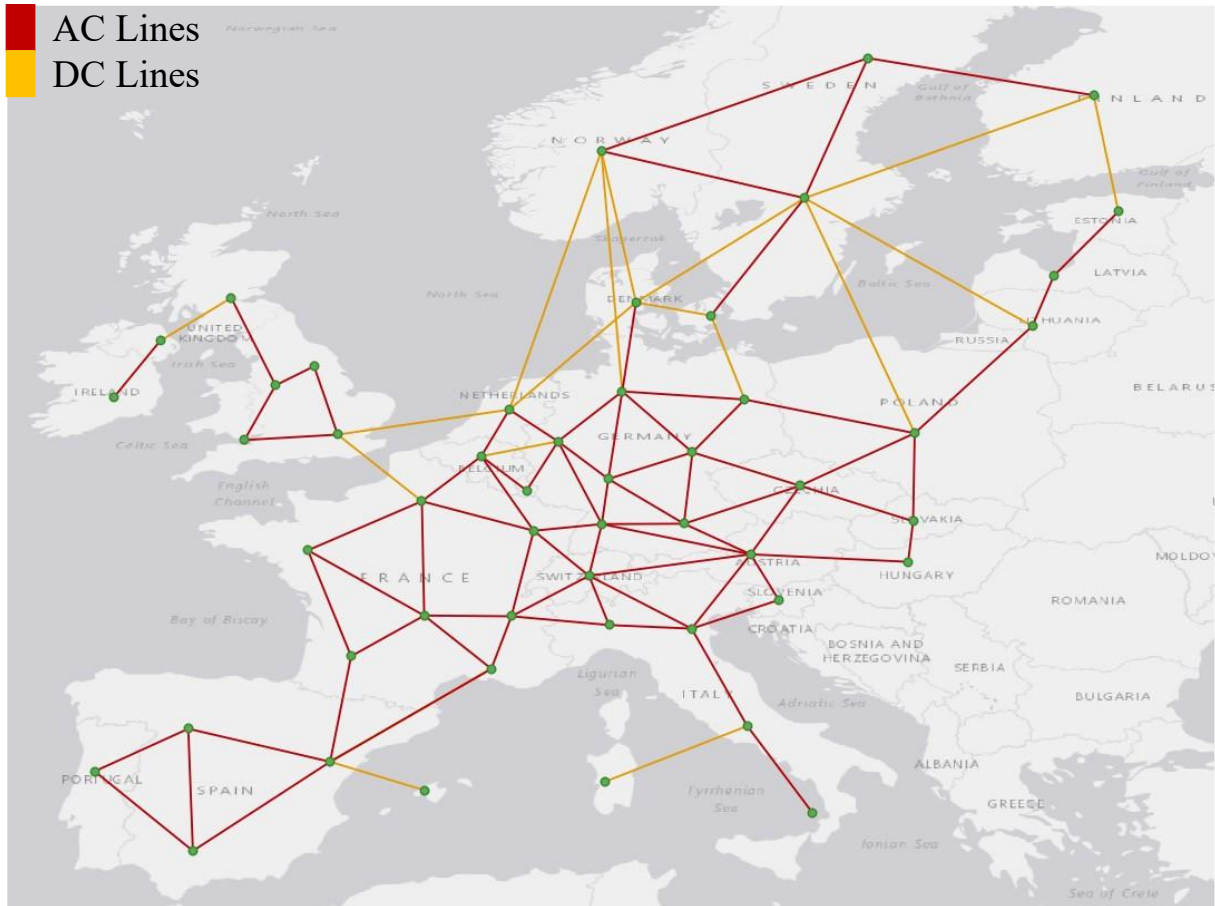


Figure 1: Map of clustered EU high-voltage electricity system – own illustration

4.1 Uncertainty Sets

To assess which combination of generation, storage, and transmission technologies ensures the robustness of a future European electricity system against worst-case realizations of low availability events, we stress-tested the expansion model using synthetic extreme weather scenarios. Our methodology for modeling these worst-case scarcity events consisted of two main steps. In the first step, we defined the geographical scope, introducing weather regions within Europe. In these regions, solar and wind availability can be modeled either as typical availability conditions or as scarcity periods consisting of extreme low availability scenarios. In the second step, we defined the uncertainty realization space by specifying the number of affected regions, using a cardinality-constrained uncertainty set. In the following, we outline our methodology, first addressing the geographic scope of the extreme scarcity events, and then describing the cardinality-constrained uncertainty set.

4.1.1 Geographical Scope

In order to incorporate the effects of weather events with low solar and wind availability, our approach relied on splitting the modeled European system into six weather regions. Therefore, we assigned 24 European countries to these regions in accordance with the study by Otero et al., (2022), as shown in Figure 2. Those authors analyzed the correlation between the monthly frequencies of energy compound events (periods with low wind and solar irradiance) among different European countries, considering the spatial relationship between critical energy events across Europe. Within these regions we assume that the weather conditions, which translate back to the nodal renewable capacity factors, are the same: normal availability or low solar availability or low wind availability, or both low solar availability and low wind availability.

³ https://github.com/bernemax/ARO_Dunkelflaute_Europe

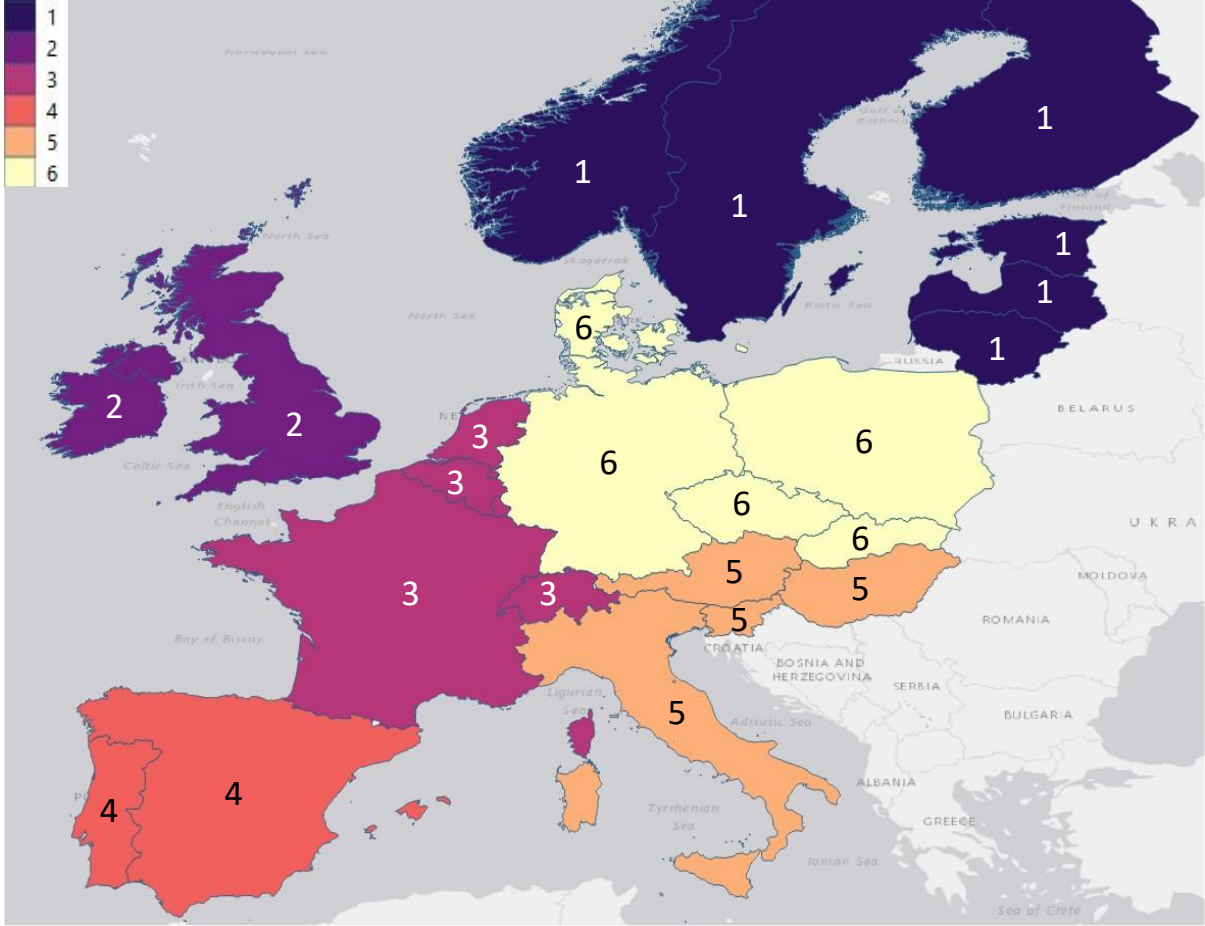


Figure 2: Map of weather regions, Region 1: NO, SE, FI, LV, LT, EE, Region 2: GB, IE, Region 3: NL, BE, FR, CH, LU, Region 4: ES, PT, Region 5: IT, AT, SI, HU, Region 6: DE, DK, CZ, PL, SK– own illustration.

4.1.2 Renewable Uncertainty - Capacity Factors Lower Bounds

In our case study, we set the renewable scarcity event duration to be one week (7 days), which corresponds also to a typical time span of a worst case Dunkelflaute event (Raynaud et al., 2018; Li et al., 2021b; Otero et al., 2022b). The uncertainty realization of such an extreme event is controlled by the uncertainty budget $\Gamma_{r,p}$ as defined in eq. (32). The budget controls the number of deviations in solar or wind availability from their reference values across the defined weather regions and time periods. Here $\Gamma_{r,p} = 0$ implies that no uncertainty occurs for the specific generation technology, meaning that the renewable capacity factor time series remains at its expected reference values for all regions. For all discrete values $\Gamma_{r,g} \geq 0$, a low renewable availability (scarcity) period can occur in a specific weather region as the deviation value $\widehat{c}f_{r,g,t}$ is subtracted from the reference value. To determine $\widehat{c}f_{r,g,t}$, we generated a synthetic low-capacity factor time series which serves as a so-called lower bound. We created this lower bound by concatenating on a week-by-week basis the availability time series that had the lowest average availability of the respective 40 weeks of the same time period. The deviation value $\widehat{c}f_{r,g,t}$ then corresponds to the difference between the reference value $\widetilde{c}f_{r,g,t}$ and the lower bound of the capacity factor. An exemplary visualization of the lower bound and the reference values for solar PV in Austria is presented in Appendix C.

4.2 Scenario Definition

Since we examine the effect of different geographical coverages of low availability events, we investigate six different ARO scenarios, by gradually increasing the uncertainty budgets Γ_{PV} and Γ_{Wind} from 1 to 6. In scenario ARON, exactly N regions experience a low-availability event for wind, and N regions experience such an event for solar PV. Accordingly, ARO1 through ARO6 represent cases with one to six affected regions, respectively. More formally, the integer number of the respective uncertainty budget represents the number of regions that can be affected by low solar PV or wind availability periods. Thus, the model endogenously decides in which region the availability is reduced. For example, in scenario ARO1, one region can be affected by low availability for both solar PV and wind, in the ARO2 scenario, the model can set the availability of solar PV and wind to the lower bound in two regions and so on, up to ARO6, where all six regions can simultaneously experience

of regions who are overly dependent on a single dominant renewable source. A robust system configuration must therefore diversify the generation mix to mitigate this exposure, as discussed in the following sections.

5.2 Robust System – Cost and Investments

Figure 4 illustrates the worst-case weather realizations for each scenario, along with the resulting total system costs of the robust solution and regional cost contributions. These outcomes represent the point at which the ARO model’s min-max optimization converges—where no further cost reductions are possible through technology adoption, and no higher objective values can be achieved through alternative uncertainty realizations.

The scenario-by-scenario comparison shows how increasing the uncertainty budget alters the geographic coverage of low-availability events. In ARO1 (top left of Figure 4), the model identifies low availability of both solar PV and wind in Region 3 as the worst-case scenario—effectively a worst-case regional *Dunkelflaute*. In ARO2 (top right), where the number of low-availability regions is increased to two, the selected regions differ from ARO1. However, Region 3 is again identified as experiencing a *Dunkelflaute*. Additionally, Region 6 faces low solar PV availability, while Region 1 experiences low wind. In ARO3, both Region 3 and Region 6 are affected by *Dunkelflaute* conditions, and Region 5 shows reduced solar PV availability. We observe that the model now selects Region 2, rather than Region 1, to experience low wind. In ARO4, low wind in Region 1 and low solar in Region 4 are added, resulting in all regions experiencing at least one type of low availability. ARO5 further includes low availability in Regions 2 and 4, and in ARO6, *Dunkelflaute* conditions simultaneously affect all six regions.

The lower part of Figure 4 shows the progression of total system costs (i.e., the model’s objective value), which includes annual investment and generation costs as defined in Equation (1) in Subsection 4.1. It also displays the average electricity cost per scenario. In the Base scenario, total system costs amount to €151 billion, with an average electricity cost of €51/MWh. In ARO1, costs rise moderately by 9 %, suggesting that the integrated European system can efficiently absorb localized renewable scarcity events. However, as more regions experience low availability, system costs increase rapidly: in ARO2, costs reach €199 billion (+31 %) with €66/MWh on average; in ARO3, they rise to €228 billion (+50 %); in ARO4, to €245 billion (+62 %); and in ARO5, to €256 billion (+70 %) with an average cost of €85/MWh. The increase in ARO6 is marginal, reaching €258.5 billion (+71 %) and €86/MWh on average. This steep rise followed by a plateau indicates a nonlinear system response, where early regional shocks are manageable, but broader events quickly exhaust cost-effective adaptation measures.

The regional cost shares in Figure 3 further illustrate how the system cost burden is distributed. Across all scenarios, Regions 3, 5, and 6 contribute the most to total system costs. Nearly all regions, except Region 6, approximately double their costs from the Base to the ARO6 scenario due to shifts in their generation mix. However, the sensitivity to scenario severity varies by region. In the early scenarios, cost increases are driven mainly by Region 6, while other regions see only modest changes. From ARO3 onward, Region 6’s costs begin to decline, while Regions 1, 3, and 5 show substantial increases. This pattern suggests that Region 6 is particularly vulnerable to smaller-scale *Dunkelflaute* events, where it must absorb the renewable shortfall on its own. As more regions are affected in later scenarios, the compensation burden is redistributed, alleviating pressure on Region 6 and helping stabilize its supply.

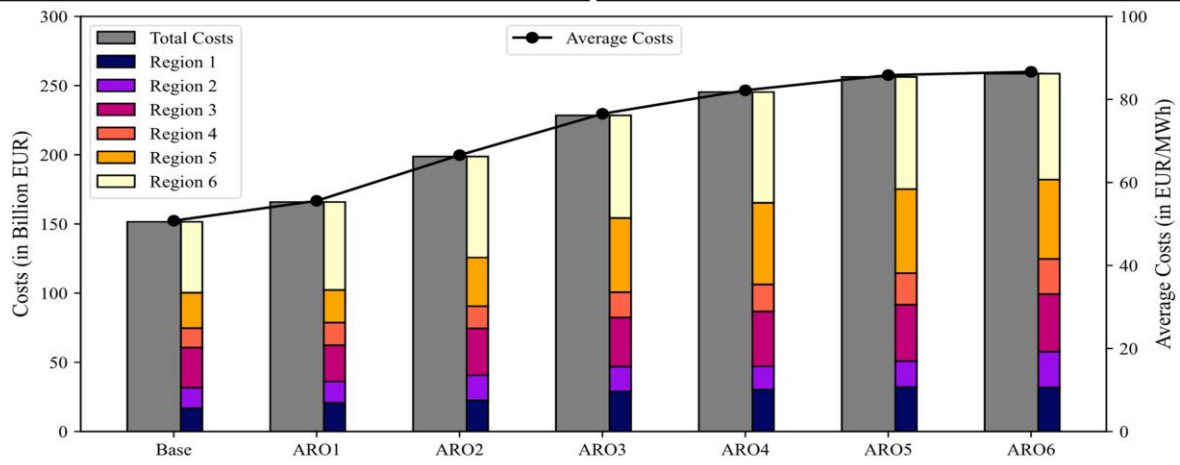
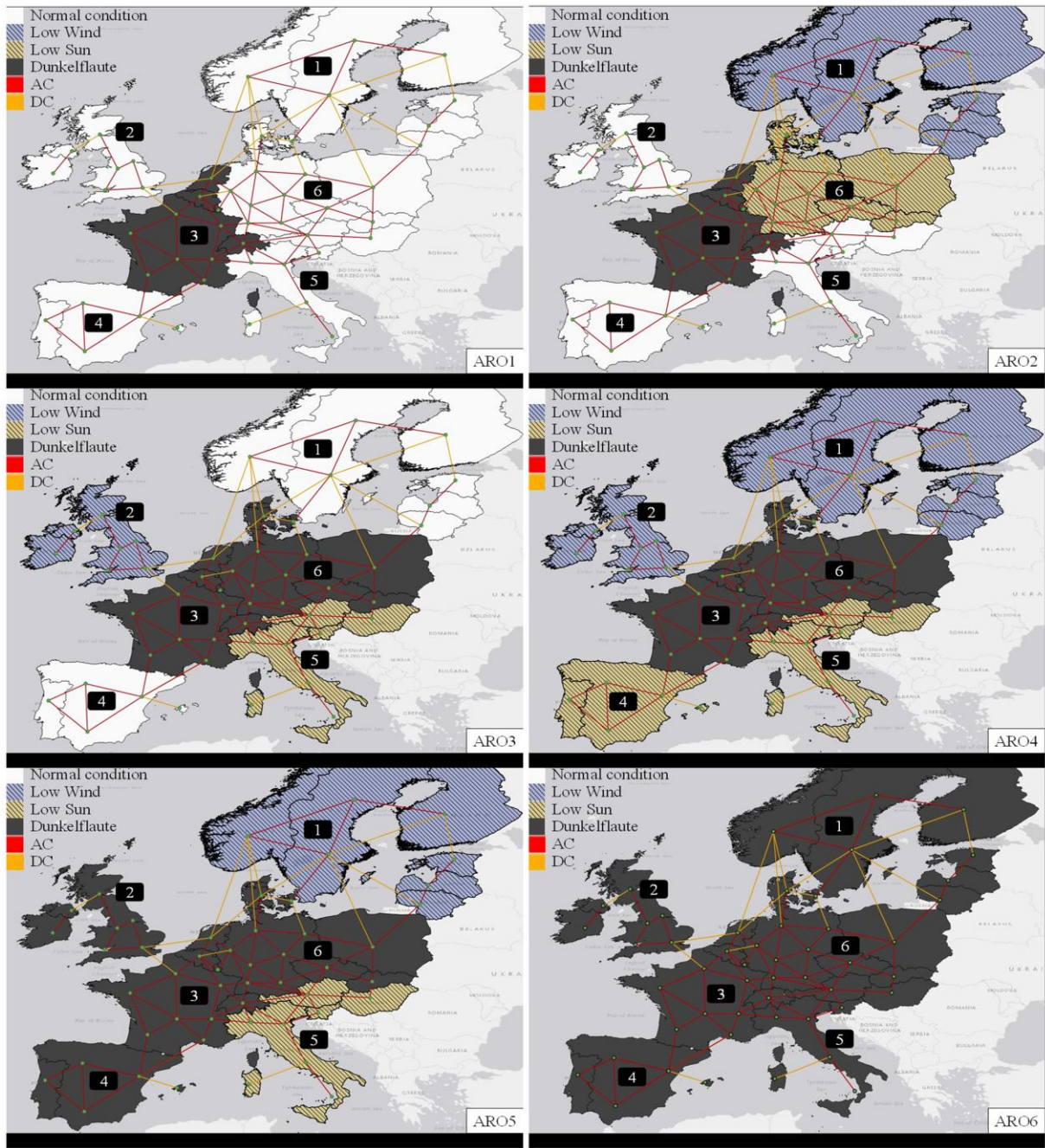


Figure 3: Scenario specific worst case regional weather realizations, maps for ARO1, ARO2, ARO3, ARO4, ARO5, ARO6, and system costs with regional shares and average electricity costs, own illustration.

Figure 4 reveals the trends in technology-specific investments. Onshore wind appears consistently across all regions, while significant solar PV deployment is concentrated in Regions 4 and 5 and, depending on the scenario, also in Regions 3 and 6. In particular, Regions 3 and 6 show more prominent solar PV investments in low-coverage scenarios (ARO1–ARO3), which decline as the number of affected regions increases in higher-coverage scenarios (ARO4–ARO5).

Additionally, we observe a substantial increase in investment cost for long-term hydrogen storage and load shedding as more regions are impacted by low availability. Hydrogen storage investments become significant starting in ARO2, especially in Regions 1, 3, 5, and 6. By ARO6, hydrogen storage accounts for 19 %–25 % of the regional system costs. Load shedding also becomes a relevant measure from ARO2 onward, with the model increasingly relying on both storage technologies and demand curtailment to meet the final megawatts of residual demand during extreme renewable scarcity events.

These findings demonstrate that the optimal robust investment mix is shaped not only by the severity of *Dunkelflaute* events but also by their regional resource endowments. In particular, long-term storage technologies emerge as critical components of the robust solution once renewable scarcity events affect a broader portion of the system.

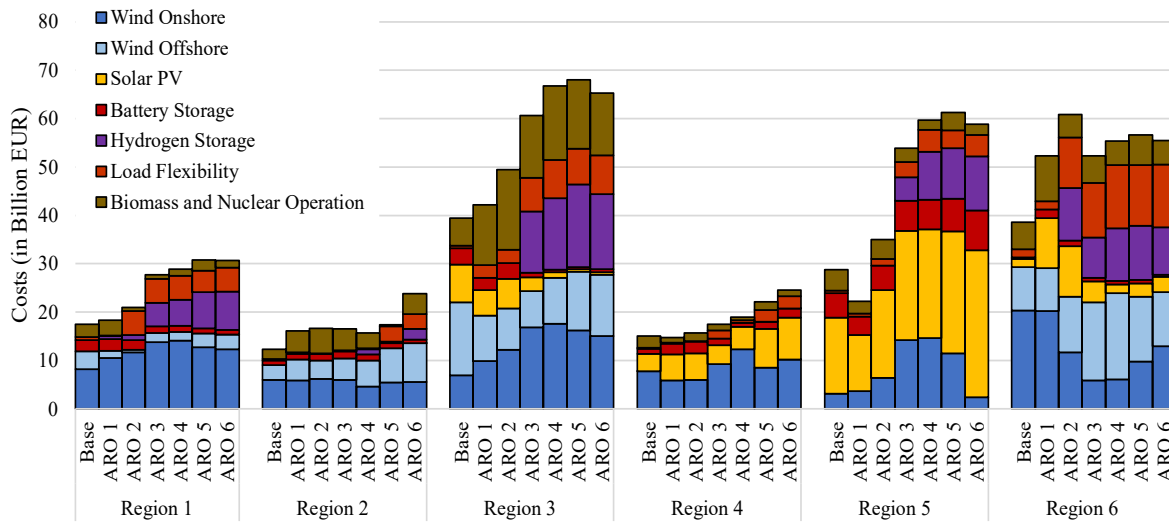


Figure 4: Regional and scenario-specific electricity investment, generation, and load shedding costs, own illustration.

5.3 Installed Capacity and Regional Generation Mix

Figure 5 depicts the scenario-specific installed capacities for each technology, aggregated across Europe. Despite its modest share in total system costs, solar PV comprises the largest share of installed capacity, reaching up to 50% across all scenarios. Wind power represents the second-largest share, with onshore wind dominating over offshore. Battery inverters form the third-largest component of installed capacity. Investments in battery inverters increase notably when one or two regions are affected by low availability events but decline and stabilize as more regions become impacted. Overall, battery deployment closely follows the pattern of solar PV investments.

In line with the cost trend, the installed capacities of hydrogen technologies, specifically electrolyzers (for charging) and H₂-fired OCGTs (for discharging), become significant from ARO3 onwards, with 66 GW of electrolyzer and 45 GW of OCGT capacity. These capacities continue to grow through ARO6, reaching approximately 98 GW of electrolyzers and 70 GW of OCGTs, together accounting for around 6% of total installed capacity. This trend reinforces the role of long-term hydrogen storage as a preferred solution for handling large-scale *Dunkelflaute* events.

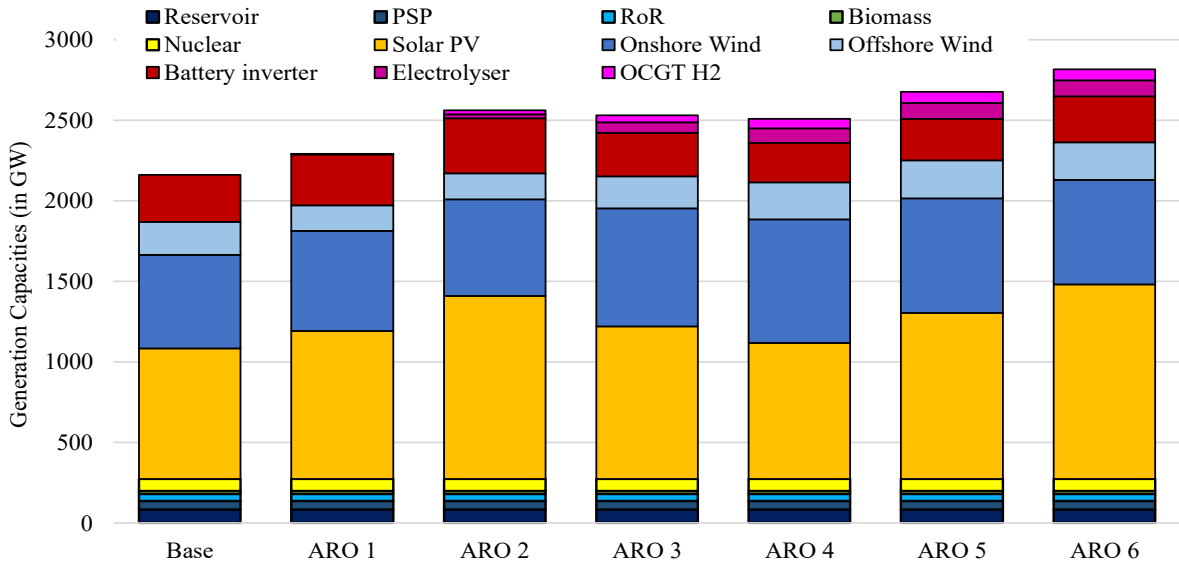


Figure 5: Scenario-specific technology capacity mix, own illustration.

Figure 6 presents the regionally differentiated, scenario-specific annual electricity generation (in TWh), alongside regional electricity demand indicated by red dotted lines. When a region’s total generation exceeds this line, it functions as a net exporter. Electricity generation is dominated by wind power in most regions, while solar PV plays a more prominent role in Southern Europe. Most regions are either net exporters or nearly self-sufficient, with the exception of Region 6, where electricity demand significantly exceeds domestic generation. When only Region 3 is affected by low availability (e.g., in ARO1), Region 6 responds with increased domestic generation investment. However, as additional regions are impacted, Region 6 reduces its investment and maintains a relatively stable generation level.

Although hydrogen technologies account for a substantial share of total system costs, their contribution to electricity generation remains modest. A similar pattern is seen with load shedding, which stays below 1% of total generation in all scenarios. This stark contrast between cost and energy output highlights the high expense of maintaining backup capacity to safeguard the system during extreme low availability periods. Identifying cost-effective, large-scale backup solutions remains a critical challenge for reducing total system costs. Detailed regional and scenario-specific analysis is provided in Appendix E.

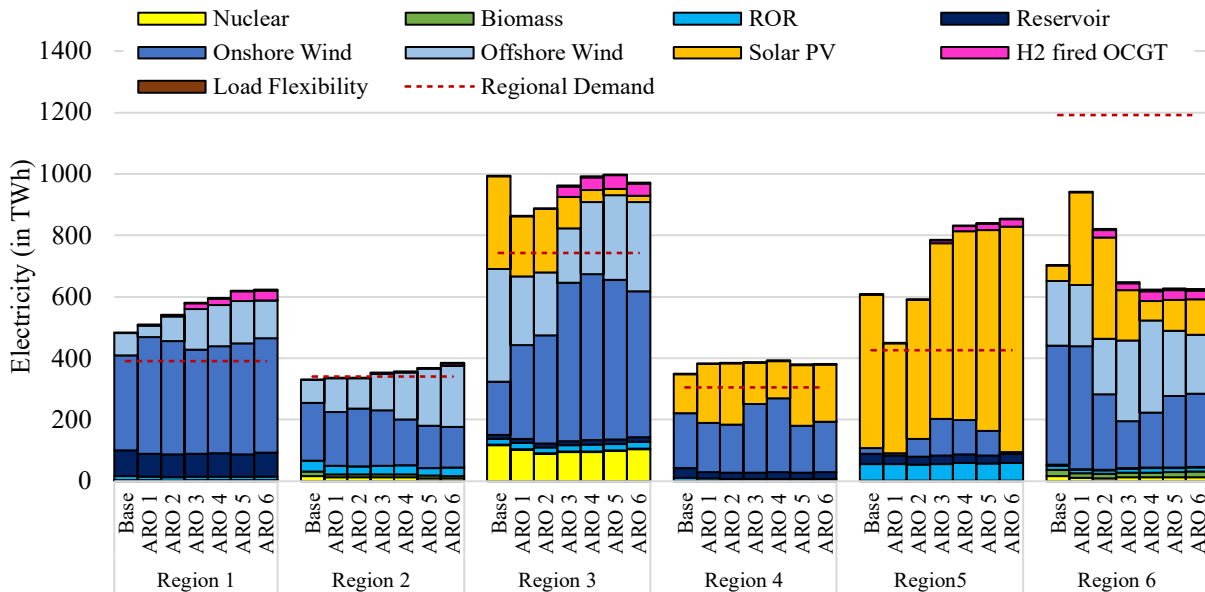


Figure 6: Regional generation mix in relation to the regional demand, own illustration.

5.4 Storage Capacity Expansion

Figure 7 presents the scenario specific regional storage capacity expansion using the storage-demand ratio on the primary as well as the total regional storage capacity on the secondary Y-axis. The storage-demand enables the comparison of storage

requirements across systems and serves as a proxy for the flexibility storage provides to the energy system. For more detailed insights on this metric, the interested reader is referred to Zerrahn et al. (2018) and to Appendix F.

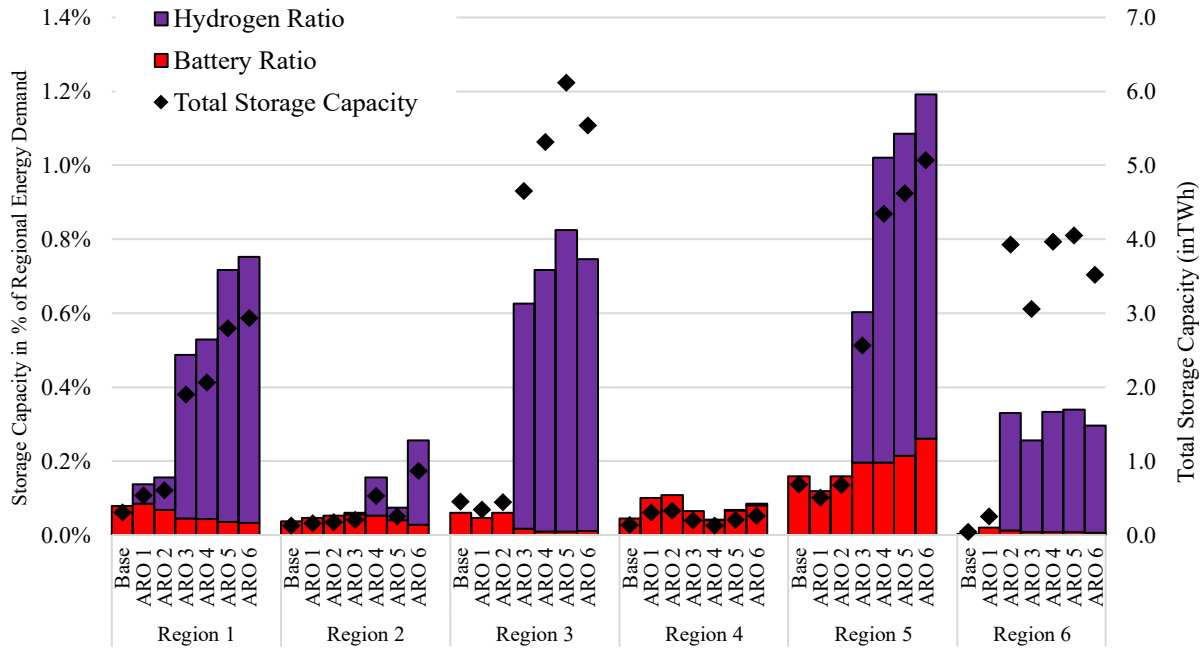


Figure 7: Regional storage-demand ratio plotted with stacked bars for battery storage capacity and hydrogen storage capacity on the primary axis, regional storage capacity plotted with black markers on the secondary axis, own illustration.

The figure presents two different findings: first, the absolute installed storage capacity shows that in the first two ARO scenarios most of the storage capacity in each region, but Region 6, comes from battery systems. As solar PV generation in Region 3 and Region 5 plays a major role, so does the battery storage capacity. Starting from the ARO2 scenario, the hydrogen storage expansion becomes significant, mainly driven by expansion in Region 1 and Region 6. Notably, in the ARO2 scenario, Region 6 significantly increases its hydrogen storage capacity, constructing more storage capacity (4 TWh) than all the other regions combined. However, from the ARO3 scenario Region 1, Region 4 and Region 5 are catching up, making Region 3 the region with the highest installed hydrogen storage capacity. For the ARO6 scenario, the hydrogen storage capacity for the system totals 16.5 TWh and the battery storage capacity 1.7 TWh. Second, the storage-demand ratio shows that storage expansion is decoupled from the region's energy demand. From the ARO3 scenario onward, Region 1, Region 3 and Region 5 built proportionally the most storage capacity to compensate for the renewable scarcity period, indicating that they require disproportionately more storage to cope with renewable scarcity periods. On the contrary, Region 2, Region 4 and Region 6 remain constantly below the average storage-demand ratio, showing on an overall system level a lower adoption sensibility against the modelled extreme. A regional comparison including the average storage-demand ratio across all regions is presented in Figure 13 in the Appendix F. To evaluate the role of long-term hydrogen storage in ensuring system stability, Table 2 presents the installed H₂-fired OCGT capacity and the maximum hydrogen storage discharge duration for the ARO6 scenario as a representative worst-case example.

Table 2: Maximum discharging capacity and duration of long-term storage in the ARO6 scenario.

Region	Region 1	Region 2	Region 3	Region 4	Region 5	Region 6
H ₂ fired OCGT in GW	11.8	4.0	24.1	0.1	16.5	13.9
Duration in hours	139	115	132	112	142	147

The table indicates that hydrogen storage is dimensioned to cover between four and six days of demand, aligning closely with the modeled seven-day renewable scarcity event duration. The capacities of both hydrogen storage and OCGT plants are optimized accordingly. Region 3 and Region 5 install the highest levels of OCGT capacity, enabling them to support not only their own loads but to also partially cover Region 6 during a renewable scarcity period. This finding is evaluated in more detail in Appendix E.

These results highlight how worst-case scarcity events identified by the model shape the regional demand for long-duration storage, revealing the cost sensitivity of different regions under stress. The earlier hydrogen storage appears in the optimal

capacity mix, the more exposed a region is to extreme events—suggesting that lower-cost options such as load flexibility, transmission, or renewable generation expansion have already been exhausted. An alternative - expanding other firm capacity like oil power plants or carbon-neutral nuclear power plants to cover the period - remains outside the scope of this analysis.

6 DISCUSSION AND CONCLUSION

This study introduces the first adaptive robust capacity expansion model that endogenously incorporates worst-case weather events into the long-term planning of a decarbonized electricity system spanning 24 European countries. A key advantage of the ARO framework lies in its sequential decision-making structure, which allows the model to anticipate and respond to the most severe realizations of weather-related uncertainty. By treating periods of low solar and wind availability as worst-case events, the model identifies their potential timing and regional occurrence, quantifies their system-wide impact, and determines the adjustments required to ensure a robust and resilient technology mix.

From a methodological perspective, this study advances the literature on robust European energy systems by introducing an optimization framework that captures the regional distribution of weather-related uncertainty and system adaptation. While existing studies assess the overall system-wide effects of weather robustness, our approach goes further by distinguishing between regional impacts related to capacity adoptions and cost developments. On this basis our model reveals region-specific adaptation strategies and vulnerabilities, emphasizing the importance of incorporating regional differentiation into robust energy system planning.

Our results reveal on a system wide (European) basis a nonlinear cost response as the geographical scope of low availability events increases. Compared to the baseline scenario (€151.6 billion), system costs rise moderately under localized shocks (+9% in ARO1), but increase sharply when broader impacts are considered (+31% in ARO2, +51% in ARO3). As more regions are affected, marginal cost increases taper off: +62 % in ARO4, +69 % in ARO5, and +71 % in ARO6. The nonlinear shape of the cost–adaptation curve reflects how the system’s ability to balance renewable scarcity events evolves as the spatial extent of these events increases. Under localized shocks (ARO1), cost increases remain modest because unaffected regions can effectively compensate through cross-border energy exchanges, requiring only limited additional storage or renewable capacity. However, as the geographical scope widens (ARO2 and ARO3), regions that previously served as balancing partners are themselves affected, sharply reducing the system’s inherent flexibility. This triggers a disproportionately large rise in system costs, driven by the need to expand storage and renewable generation to shift surplus energy into scarcity periods. Once most regions are already impacted (ARO4–ARO6), the cost curve begins to flatten: much of the necessary long-duration storage and excess generation has already been built, and the remaining shortfalls can be compensated more easily within the newly affected regions themselves. As a result, marginal adaptation costs decline, and the curve approaches a saturation point.

Comparison with previous studies shows that ARO1 aligns closely with deterministic models such as Gøtske et al. (2024) and Grochowiec et al. (2024) while ARO2 yields results similar to those of Plaga and Bertsch (2022). The significantly higher costs observed in ARO3 and beyond likely stem from our model design, which combines multiple worst-case events and enforces a strict carbon cap, excluding other low-carbon backup options such as nuclear power, and incorporates relatively high costs for load shedding. While these assumptions may yield conservative estimates, they enable us to explore the upper bounds of system cost escalation and to identify the technologies required to hedge against large-scale Dunkelflaute events across Europe. Furthermore, the results underscore the strong sensitivity of system configurations to the geographic scope of such extreme events. This emphasizes the need for system operators and policymakers to develop a clear understanding of which types of events to anticipate. Consequently, harmonizing assumptions regarding extreme weather scenarios is a key prerequisite for planning a weather-resilient European energy system.

At the regional level, our results provide insights into which regions are mostly affected by worst-case renewable scarcity events and how the cost increases associated with a broader geographic extent of these events are distributed across regions. We identify which regions contribute most to overall system costs and demonstrate how the burden of adaptation shifts—from central regions under localized events to more peripheral regions as the spatial coverage of the scarcity event expands.

The ARO model consistently identifies central European regions, particularly Regions 3 and 6, as critical. Region 6, which encompasses major demand centers like Germany, relies on imports from Region 3, a strong renewable producer. When either is affected by low availability, the cost of reconfiguring the system increases substantially. In contrast, peripheral regions (e.g., Regions 1, 2, 4, and 5) are less frequently identified as critical extreme event locations but still face high adaptation costs when central regions are impacted. This is particularly evident for Regions 1 and Region 5, which disproportionately expand their storage infrastructure to help maintain overall system balance. Beginning with the ARO-3 scenario, both regions consistently exhibit a storage-to-demand ratio well above the systemwide average, whereas other regions, most notably Region 6, show ratios below the average. These findings underscore the practical relevance of a coordinated European energy policy. While

central European countries benefit from a system-wide optimization perspective, peripheral countries may face higher system cost. Ongoing debates in countries such as Norway⁵ and Sweden⁶ - where high electricity prices have been attributed to exports during periods of renewable scarcity, particularly to neighboring countries like Denmark and Germany - illustrate the emerging tensions. These developments serve as an early indication of the distributional challenges that may intensify as Europe transitions toward a fully renewable electricity system. To avoid future fragmentation and resource nationalism driven by national priorities, our work demonstrates that a robust system on a European scale might be cost efficient in handling extreme renewable scarcity events, while on a local or regional scale the cost burdens are unevenly distributed. To promote social and political acceptance policymakers should not only incentivize investments in renewables, transmission infrastructure, and storage in high-potential regions, but also consider cross-border cost compensation or benefit-sharing mechanisms.

Another key insight is the shift in optimal system configuration as the geographical scale of the renewable scarcity event grows. For small-scale events (ARO1, ARO2), expanding renewables, batteries, and transmission capacity is cost-effective. But as interregional balancing becomes constrained by widespread weather events, long-term hydrogen storage becomes essential. Although hydrogen accounts for a large share of system costs, its actual contribution to electricity generation remains modest. Likewise, load shedding remains under 1% of total generation in all scenarios but still significantly drives system costs, highlighting the need for affordable, large-scale backup capacity.

A limitation of this study lies in the representation of weather data. First, we use a synthetic average weather year rather than a historical one for the Base scenario. While this approach captures representative renewable generation patterns, it may not fully reflect the variability and temporal extremes found in real-world data. Second, to reduce computational complexity, we apply a time series reduction technique using a four-hour moving average. This smoothing may underestimate the intensity and frequency of short-lived extreme events. Third, the model assumes static, predefined weather regions for the realization of extreme events, which does not reflect the continuous and dynamic nature of real weather systems. In reality, low availability conditions can span irregular and shifting geographical areas. Fourth, the model focuses exclusively on seven-day periods of low solar and wind availability, with uncertainty realizations restricted to a four-week window in January. As a result, extreme events occurring in other months or with different durations are not captured. These assumptions may lead to an underestimation of required year-round storage requirement, especially for seasonal storage systems.

Additional model limitations include fixed capacities for firm generation technologies (e.g., nuclear), which are based on current levels or policy targets, and constraints on transmission expansion. Allowing these capacities to expand endogenously or without limits could lead to different investment strategies. We also do not account for the hydrogen sector, omitting the additional system flexibility of the hydrogen transportation and storage infrastructure. This may lead to an overestimation of the modelled extreme events on the overall system costs. Finally, our results are subject to the 2050 technology cost projections. Different cost developments may lead to other optimal system configurations.

7 ACKNOWLEDGEMENTS

Maximilian Bernecker gratefully acknowledges supported by the Federal Ministry of Education and Research, Award No. 19FS2032C, as well as the German Federal Government, the Federal Ministry of Education and Research, and the State of Brandenburg within the framework of the joint project EIZ: Energy Innovation Center (project numbers 85056897 and 03SF0693A) with funds from the Structural Development Act (Strukturstärkungsgesetz) for coal-mining regions.”

Felix Müsgens gratefully acknowledges financial support from the Federal Ministry of Education and Research of Germany in the Ariadne project (03SFK5S0).

Igor Riepin acknowledges support by the German Federal Ministry for Economic Affairs and Energy (BMWE) under Grant No. 03E14083A (RESILIENT) jointly with the CETPartnership through the Joint Call 2022. As such, I.R. further acknowledges funding from the European Union’s Horizon Europe research and innovation programme under grant agreement no. 101069750.

⁵ <https://www.euronews.com/business/2024/12/13/norway-aims-to-cut-energy-links-with-europe-due-to-soaring-prices>

⁶ <https://harici.com.tr/en/sweden-blames-germanys-nuclear-phase-out-for-energy-crisis/>

8 OPEN DATA STATEMENT

The model is formulated using the General Algebraic Modeling Language (GAMS). The code and data are available at github: https://github.com/bernemax/ARO_Dunkelflaute_Europe

9 REFERENCES

- Baringo, L., Boffino, L., Oggioni, G., 2020. Robust expansion planning of a distribution system with electric vehicles, storage and renewable units. *Applied Energy* 265, 114679. <https://doi.org/10.1016/j.apenergy.2020.114679>
- Baringo, L., Rahimiyan, M., 2020. *Virtual Power Plants and Electricity Markets: Decision Making Under Uncertainty*. Springer International Publishing, Cham. <https://doi.org/10.1007/978-3-030-47602-1>
- Beck-Bang, A.C., Overgaard, S.B., Keles, D., 2026. Electricity supply and demand in the European market: the effect on generation adequacy in a dunkelflaute period. *Energy Policy* 208, 114910. <https://doi.org/10.1016/j.enpol.2025.114910>
- Bertsimas, D., Litvinov, E., Sun, X.A., Zhao, J., Zheng, T., 2013. Adaptive Robust Optimization for the Security Constrained Unit Commitment Problem. *IEEE Trans. Power Syst.* 28, 52–63. <https://doi.org/10.1109/TPWRS.2012.2205021>
- Bertsimas, D., Sim, M., 2004. The Price of Robustness. *Operations Research* 52, 35–53. <https://doi.org/10.1287/opre.1030.0065>
- Bloomfield, Hannah C., Brayshaw, D.J., Charlton-Perez, A.J., 2020. Characterizing the winter meteorological drivers of the European electricity system using targeted circulation types. *Meteorological Applications* 27, e1858. <https://doi.org/10.1002/met.1858>
- Bloomfield, H. C., Suitters, C.C., Drew, D.R., 2020. Meteorological Drivers of European Power System Stress. *Journal of Renewable Energy* 2020, e5481010. <https://doi.org/10.1155/2020/5481010>
- Brown, T., Schlachtberger, D., Kies, A., Schramm, S., Greiner, M., 2018. Synergies of sector coupling and transmission reinforcement in a cost-optimised, highly renewable European energy system. *Energy* 160, 720–739. <https://doi.org/10.1016/j.energy.2018.06.222>
- Caglayan, D.G., Heinrichs, H.U., Robinius, M., Stolten, D., 2021. Robust design of a future 100% renewable european energy supply system with hydrogen infrastructure. *International Journal of Hydrogen Energy, HYDROGEN ENERGY SYSTEMS* 46, 29376–29390. <https://doi.org/10.1016/j.ijhydene.2020.12.197>
- Conejo, A.J., Baringo Morales, L., Kazempour, S.J., Siddiqui, A.S., 2016. *Investment in Electricity Generation and Transmission*. Springer International Publishing, Cham. <https://doi.org/10.1007/978-3-319-29501-5>
- Conejo, A.J., Wu, X., 2022. Robust optimization in power systems: a tutorial overview. *Optim Eng* 23, 2051–2073. <https://doi.org/10.1007/s11081-021-09667-3>
- Davis, S.J., Lewis, N.S., Shaner, M., Aggarwal, S., Arent, D., Azevedo, I.L., Benson, S.M., Bradley, T., Brouwer, J., Chiang, Y.-M., Clack, C.T.M., Cohen, A., Doig, S., Edmonds, J., Fennell, P., Field, C.B., Hannegan, B., Hodge, B.-M., Hoffert, M.I., Ingersoll, E., Jaramillo, P., Lackner, K.S., Mach, K.J., Mastrandrea, M., Ogden, J., Peterson, P.F., Sanchez, D.L., Sperling, D., Stagner, J., Trancik, J.E., Yang, C.-J., Caldeira, K., 2018. Net-zero emissions energy systems. *Science* 360, eaas9793. <https://doi.org/10.1126/science.aas9793>
- Gøtske, E.K., Andresen, G.B., Neumann, F., Victoria, M., 2024. Designing a sector-coupled European energy system robust to 60 years of historical weather data. *Nat Commun* 15, 10680. <https://doi.org/10.1038/s41467-024-54853-3>
- Grochowicz, A., Greevenbroek, K. van, Benth, F.E., Zeyringer, M., 2023. Intersecting near-optimal spaces: European power systems with more resilience to weather variability. *Energy Economics* 106496. <https://doi.org/10.1016/j.eneco.2022.106496>
- Grochowicz, A., van Greevenbroek, K., Bloomfield, H.C., 2024. Using power system modelling outputs to identify weather-induced extreme events in highly renewable systems. *Environ. Res. Lett.* 19, 054038. <https://doi.org/10.1088/1748-9326/ad374a>
- Jabr, R.A., 2013. Robust Transmission Network Expansion Planning With Uncertain Renewable Generation and Loads. *IEEE Trans. Power Syst.* 28, 4558–4567. <https://doi.org/10.1109/TPWRS.2013.2267058>
- Jurasz, J., Mikulik, J., Dąbek, P.B., Guezgouz, M., Kaźmierczak, B., 2021. Complementarity and ‘Resource Droughts’ of Solar and Wind Energy in Poland: An ERA5-Based Analysis. *Energies* 14, 1118. <https://doi.org/10.3390/en14041118>
- Li, B., Basu, S., Watson, S.J., Russchenberg, H.W.J., 2021a. A Brief Climatology of Dunkelflaute Events over and Surrounding the North and Baltic Sea Areas. *Energies* 14, 6508. <https://doi.org/10.3390/en14206508>
- Li, B., Basu, S., Watson, S.J., Russchenberg, H.W.J., 2021b. Mesoscale modeling of a “Dunkelflaute” event. *Wind Energy* 24, 5–23. <https://doi.org/10.1002/we.2554>

- Li, B., Basu, S., Watson, S.J., Russchenberg, H.W.J., 2020. Quantifying the Predictability of a ‘Dunkelflaute’ Event by Utilizing a Mesoscale Model. *J. Phys.: Conf. Ser.* 1618, 062042. <https://doi.org/10.1088/1742-6596/1618/6/062042>
- Mattsson, N., Verendel, V., Hedenus, F., Reichenberg, L., 2021. An autopilot for energy models – Automatic generation of renewable supply curves, hourly capacity factors and hourly synthetic electricity demand for arbitrary world regions. *Energy Strategy Reviews* 33, 100606. <https://doi.org/10.1016/j.esr.2020.100606>
- Mayer, M.J., Biró, B., Szücs, B., Aszódi, A., 2023. Probabilistic modeling of future electricity systems with high renewable energy penetration using machine learning. *Applied Energy* 336, 120801. <https://doi.org/10.1016/j.apenergy.2023.120801>
- Mínguez, R., García-Bertrand, R., 2016. Robust transmission network expansion planning in energy systems: Improving computational performance. *European Journal of Operational Research* 248, 21–32. <https://doi.org/10.1016/j.ejor.2015.06.068>
- Ohlendorf, N., Schill, W.-P., 2020. Frequency and duration of low-wind-power events in Germany. *Environ. Res. Lett.* 15, 084045. <https://doi.org/10.1088/1748-9326/ab91e9>
- Otero, N., Martius, O., Allen, S., Bloomfield, H., Schaeffli, B., 2022a. Characterizing renewable energy compound events across Europe using a logistic regression-based approach. *Meteorological Applications* 29, e2089. <https://doi.org/10.1002/met.2089>
- Otero, N., Martius, O., Allen, S., Bloomfield, H., Schaeffli, B., 2022b. A copula-based assessment of renewable energy droughts across Europe. *Renewable Energy* 201, 667–677. <https://doi.org/10.1016/j.renene.2022.10.091>
- Perera, A.T.D., Nik, V.M., Chen, D., Scartezzini, J.L., Hong, T., 2020. Quantifying the impacts of climate change and extreme climate events on energy systems. *Nature Energy* 5, 150–159. <https://doi.org/10.1038/s41560-020-0558-0>
- Plaga, L.S., Bertsch, V., 2022. Robust planning of a European Electricity System under climate uncertainty, in: 2022 18th International Conference on the European Energy Market (EEM). Presented at the 2022 18th International Conference on the European Energy Market (EEM), pp. 1–8. <https://doi.org/10.1109/EEM54602.2022.9921057>
- Raynaud, D., Hingray, B., François, B., Creutin, J.D., 2018. Energy droughts from variable renewable energy sources in European climates. *Renewable Energy* 125, 578–589. <https://doi.org/10.1016/j.renene.2018.02.130>
- Reichenberg, L., Hedenus, F., Odenberger, M., Johnsson, F., 2018. The marginal system LCOE of variable renewables – Evaluating high penetration levels of wind and solar in Europe. *Energy* 152, 914–924. <https://doi.org/10.1016/j.energy.2018.02.061>
- Riepin, I., Schmidt, M., Baringo, L., Müsgens, F., 2022. Adaptive robust optimization for European strategic gas infrastructure planning. *Applied Energy* 324, 119686. <https://doi.org/10.1016/j.apenergy.2022.119686>
- Rogelj, J., Luderer, G., Pietzcker, R.C., Kriegler, E., Schaeffer, M., Krey, V., Riahi, K., 2015. Energy system transformations for limiting end-of-century warming to below 1.5 °C. *Nature Clim Change* 5, 519–527. <https://doi.org/10.1038/nclimate2572>
- Roldán, C., García-Bertrand, R., Mínguez, R., 2020. Robust transmission expansion planning with uncertain generations and loads using full probabilistic information. *Electric Power Systems Research* 189, 106793. <https://doi.org/10.1016/j.epsr.2020.106793>
- Roldan, C., Mínguez, R., García-Bertrand, R., Arroyo, J.M., 2019. Robust Transmission Network Expansion Planning Under Correlated Uncertainty. *IEEE Trans. Power Syst.* 34, 2071–2082. <https://doi.org/10.1109/TPWRS.2018.2889032>
- Roldán, C., Sánchez de la Nieta, A.A., García-Bertrand, R., Mínguez, R., 2018. Robust dynamic transmission and renewable generation expansion planning: Walking towards sustainable systems. *International Journal of Electrical Power & Energy Systems* 96, 52–63. <https://doi.org/10.1016/j.ijepes.2017.09.021>
- Ruhnau, O., Qvist, S., 2022. Storage requirements in a 100% renewable electricity system: extreme events and inter-annual variability. *Environmental Research Letters* 17, 044018. <https://doi.org/10.1088/1748-9326/ac4dc8>
- Schlachtberger, D.P., Brown, T., Schramm, S., Greiner, M., 2017. The benefits of cooperation in a highly renewable European electricity network. *Energy* 134, 469–481. <https://doi.org/10.1016/j.energy.2017.06.004>
- Wiel, K.V.D., Bloomfield, H.C., Lee, R.W., Stoop, L.P., Blackport, R., Screen, J.A., Selten, F.M., 2019. The influence of weather regimes on European renewable energy production and demand. *Environmental Research Letters* 14. <https://doi.org/10.1088/1748-9326/ab38d3>
- Yue, X., Pye, S., DeCarolis, J., Li, F.G.N., Rogan, F., Gallachóir, B.Ó., 2018. A review of approaches to uncertainty assessment in energy system optimization models. *Energy Strategy Reviews* 21, 204–217. <https://doi.org/10.1016/j.esr.2018.06.003>
- Zerrahn, A., Schill, W.-P., Kemfert, C., 2018. On the economics of electrical storage for variable renewable energy sources. *European Economic Review* 108, 259–279. <https://doi.org/10.1016/j.eurocorev.2018.07.004>
- Zhang, X., Conejo, A.J., 2018. Robust Transmission Expansion Planning Representing Long- and Short-Term Uncertainty. *IEEE Trans. Power Syst.* 33, 1329–1338. <https://doi.org/10.1109/TPWRS.2017.2717944>

APPENDIX A

Expansion Planning and Adaptive Robust Optimization

In general, expansion problems address the need to plan how future demand can be met with scarce resources, and they aim to either maximize or minimize the objective criteria under certain technical constraints. In the context of the electrical energy system, the aim is to identify how future energy needs can be met, investing in generation assets and transmission lines to meet the demand (Conejo et al., 2016). A typical optimization problem from a central planner's perspective could look like the following:

$$\begin{aligned}
 & \text{(i) } \text{Min}_x \quad IC^T x \\
 & \text{s.t.} \\
 & \quad h(x) = 0 \\
 & \quad g(x) \leq 0
 \end{aligned}$$

The objective function (i) minimizes the total system costs, which are the product of a vector x , representing an investment decision and the investment cost vector IC^T . In addition, certain equality conditions $h(x)$, such as supply, need to meet demand, and inequality conditions $g(x)$, such as that the generation is limited to the nominal capacity, must be satisfied. This problem formulation enables uncertainty to be incorporated exogenously by changing uncertain parameters and formulating deterministic scenarios, analyzing the results ex-post. On the contrary, adaptive robust optimization incorporates uncertainty in an endogenous manner, thus adding two extra layers of complexity. The aim of the robust optimization approach is to find model solutions that are immune to the worst-case uncertain perturbations within their predefined confidence bounds. In what follows, we refer to this solution as the robust solution. In ARO problems, decisions are modeled beyond this with recourse, making the solution robust to all combinations of uncertainty defined by a so-called uncertainty budget. This strategy results in a three-level optimization problem which can be formulated as follows:

$$\begin{array}{lll}
 \text{(i) } \text{Min}_x \quad IC^T x & \text{(ii) } \text{Max}_u & \text{(iii) } \text{Min}_y \quad [OC(x, u)]^T y \\
 \text{s.t.} & \text{s.t.} & \text{s.t.} \\
 h(x) = 0 & u \in U & y \in \Omega(x, u) = \{ \\
 g(x) \leq 0 & & A(x, u)y = b(x, u): \lambda \\
 & & D(x, u)y \geq e(x, u): \mu \}
 \end{array}$$

Here, the deterministic problem (i) represents solely the first stage of the optimization process, thus minimizing the system costs prior to the uncertainty realization. Based on this solution, the second level (ii) aims to maximize the total system costs by finding the worst-case realizations, represented by the variable vector u . The second-stage decision variable is bounded by the confidence bounds of the possible uncertainty realization space U , which could be, for example, the “on” or “off” status of a power plant. The third level encompasses the corrective actions, aiming to minimize total system operation costs OC based on the prior results (x, u) of level (i) and (ii). These actions are represented by variable vector y , and bounded by the feasibility space $\Omega(x, u)$ which is the constraining level (iii) based on (i) and (ii). Consequently, A, B, D, e are matrices with constant parameters and λ and μ represent the dual variables associated with equality and inequality constraints. In the context of the electricity energy system model, these actions would correspond to, for example, technical constraints of power plants in the dispatch process. This problem structure enables the model to address uncertainty endogenously, following the typical chronological order of decision making, uncertainty realization, and reaction in an infrastructure planning process (Ruiz and Conejo, 2015).

Modeling Uncertainty

To model uncertainty in the second-level problem (ii), we employ polyhedral uncertainty sets, introduced by Bertsimas and Sim (2004). More specifically, we use a cardinality-constrained polyhedral uncertainty set, which allows us to adjust the level of robustness, by controlling the number of uncertain coefficient perturbations within a constraint. This number is represented by the so-called uncertainty budget Γ , which guarantees that the solution of the model is protected against all cases up to Γ coefficients that can deviate from their nominal value.

In our second-level problem, the uncertainty is represented by the decision variable u , which can take values within specified confidence bounds:

$$u \in \{\tilde{u} - \hat{u}, \tilde{u} + \hat{u}\}$$

Here, \tilde{u} and \hat{u} are specifying the expected nominal value and the maximum deviation value. We follow the definition of the cardinality-constrained uncertainty set Ω as described by Mínguez and García-Bertrand (2016) and Baringo et al. (2020):

$$\Omega = \left\{ \begin{array}{l} u = \tilde{u} + \text{diag}(z^+) \hat{u} - \text{diag}(z^-) \hat{u}, \\ z^+, z^- \in \{0,1\}^n, \\ \sum_{k=1}^n (z^+ + z^-) \leq \Gamma \\ z^+ + z^- \leq 1 \end{array} \right\}$$

Here, the value of u depends on the binary variables z^+, z^- , which decide whether u deviates from its nominal value towards the upper or lower bound, or not. To control the level of robustness, Γ is restricting the number of deviations. A value of $\Gamma = 0$ leads to the realization of the expected value $u = \tilde{u}$, while any other discrete positive value of Γ implies that u can deviate from the expected value, which represents an uncertainty realization. Hence, u cannot take values of the upper and lower bounds at the same time, and the simultaneous realization of z^+ and z^- is excluded.

Solution Strategy

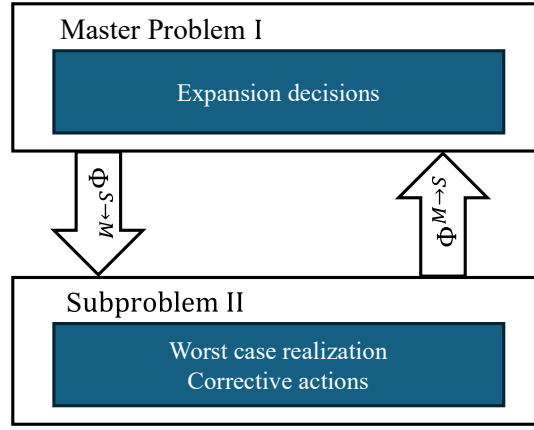


Figure 8. Iterative ARO solution approach, based on the work of Baringo et al. (2020).

The solution strategy on solving the three-level optimization problem is based on the literature stream established by Bertsimas et al. (2013), Mínguez and García-Bertrand (2016), Zhang and Conejo (2018), and Baringo et al. (2020). The first step is to couple the second level (ii) and the third level (iii) of the optimization problem, making it a single optimization problem. The second step is to linearize the new second level, and employ a column and constraint algorithm to solve the remaining two-level optimization problem in an efficient manner as visualized by Figure 8. In the following, we provide a short explanation of these processes. However, the interested reader is referred to the work of Baringo and Rahimiyan (2020) and Riepin et al. (2022) which provide a more detailed explanation.

In order to couple the third level (iii) with the second level (ii) optimization problem, we assume that problem (iii) is linear, and thus convex. On this basis we know that the dual problem solution equals the primary problem (strong duality). The reformulation of the third-level problem into its dual pendant (iii') is shown in the following:

$$\begin{array}{ll} \text{(iii)} \text{ Min}_y [OC(x, u)]^T y & \text{(iii')} \text{ Max}_{\lambda, \mu} B(x, u) \cdot \lambda + E(x, u) \cdot \mu \\ \text{s.t.} & \text{s.t.} \\ y \in \Omega(x, u) = \{ & A(x, u) \cdot \lambda + D(x, u) \cdot \mu = OC(x, u) \\ A(x, u)y = b(x, u): \lambda & \lambda: \text{free}, \mu \geq 0 \\ D(x, u)y \geq e(x, u): \mu \} & \end{array}$$

As a next step, the dual reformulated problem (iii') is merged with level (ii), resulting in a single optimization problem (II). The new two-level min (I) – max (II) optimization problem is as stated below:

$$(I) \text{Min}_x IC^T x$$

s.t.

$$h(x) = 0$$

$$g(x) \leq 0$$

$$(II) \text{Max}_{u,\lambda,\mu} [b(x,u)]^T \lambda + [D(x,u)]^T \mu$$

s.t.

$$A(x,u)\lambda + D(x,u)\mu = OC(x,u)$$

$$u \in U, \lambda : \text{free}, \mu \geq 0$$

As there is a bilinear term $[b(x,u)]^T \lambda$ in the objective function of the subproblem (II), it makes this formulation a Mixed-Integer Nonlinear Programming (MINLP) and thus is hard to solve. Therefore, big-M constraints are employed to reformulate this term, adding an auxiliary variable, making the problem a Mixed-Integer Linear Programming (MILP), which is easier to solve.

APPENDIX B

Table 3: Load shedding costs

Load shedding			
Parameter	Value	Parameter	Value
f^{L1}	5%	sc_n^{LS1}	1.000 EUR/MWh
f^{L2}	15%	sc_n^{LS2}	3.000 EUR/MWh
f^{L3}	80%	sc_n^{LS3}	12.000 EUR/MWh (1)

(1): Note that such a high load shedding level may represent an unrealistic assumption. We opted for such high value to capture anticipated future load flexibility options that may play a bigger role reducing storage capacity requirements.

Table 4: Technology data

Technology	Lifetime in years	Interest Rate	Overnight costs	Fixed OM costs	Fuel Costs	Efficiency	Data Source
Onshore Wind	30	7.5%	963 EUR/kW	9.63 EUR/kW/y	-	-	Danish Energy Agency
Offshore Wind	30	9.3%	1380 EUR/kW	13.80 EUR/kW/y	-	-	Danish Energy Agency
Solar PV	35	6.9%	370 EUR/kW	7.40 EUR/kW/y	-	-	Danish Energy Agency
Battery Inverter	10	6.0%	60.0 EUR/kW	0.6 EUR/kW/y	-	96%	Danish Energy Agency
Battery Storage	30	6.0%	75 EUR/kWh	0.6 EUR/kWh/y	-	-	Danish Energy Agency
Electrolyzer	25	8.0%	350 EUR/kW	14 EUR/kW/y	-	70%	Danish Energy Agency

H ₂ Storage Tank	30	8.0%	21 EUR/kWh	0.5 EUR/kWh/y	-	-	Danish Energy Agency
H ₂ -fired OCGT	25	8.0%	411 EUR/kW	8.7 EUR/kW/y	-	43%	Danish Energy Agency
AC Transmission	40	6.0%	700-2500 EUR/MW/km	-	-	-	NEP 2023 (1)-
DC Transmission	40	6.0%	2500-5500 EUR/MW/km	-	-	-	NEP 2023 (1)-
Biomass	60	-	-	80 EUR/kW/y	4.5 EUR/MWh th	47 %	DIW (2)
Nuclear	60	-	-	100 EUR/kW/y	3 EUR/MWh th	33 %	DIW (2)
Run of River	-	-	-	35 EUR/kW/y	-	-	DIW (2), IEA
Pumping Storage	-	-	-	45 EUR/kW/y	-	-	DIW (2), IEA
Reservoir	-	-	-	40 EUR/kW/y	-	-	DIW (2), IEA

- (1) 50Hertz Transmission GmbH, Amprion GmbH, TenneT TSO GmbH & TransnetBW GmbH. (2023). Netzentwicklungsplan Strom 2037/2045 (2023): https://www.netzentwicklungsplan.de/sites/default/files/2023-03/230321_NEP_Kostenschaetzung_NEP2037_2045_V2023_1.Entwurf.pdf
- (2) : DIW (2013): Current and prospective costs of electricity generation until 2050, https://www.diw.de/documents/publikationen/73/diw_01.c.424566.de/diw_datadoc_2013-068.pdf

APPENDIX C

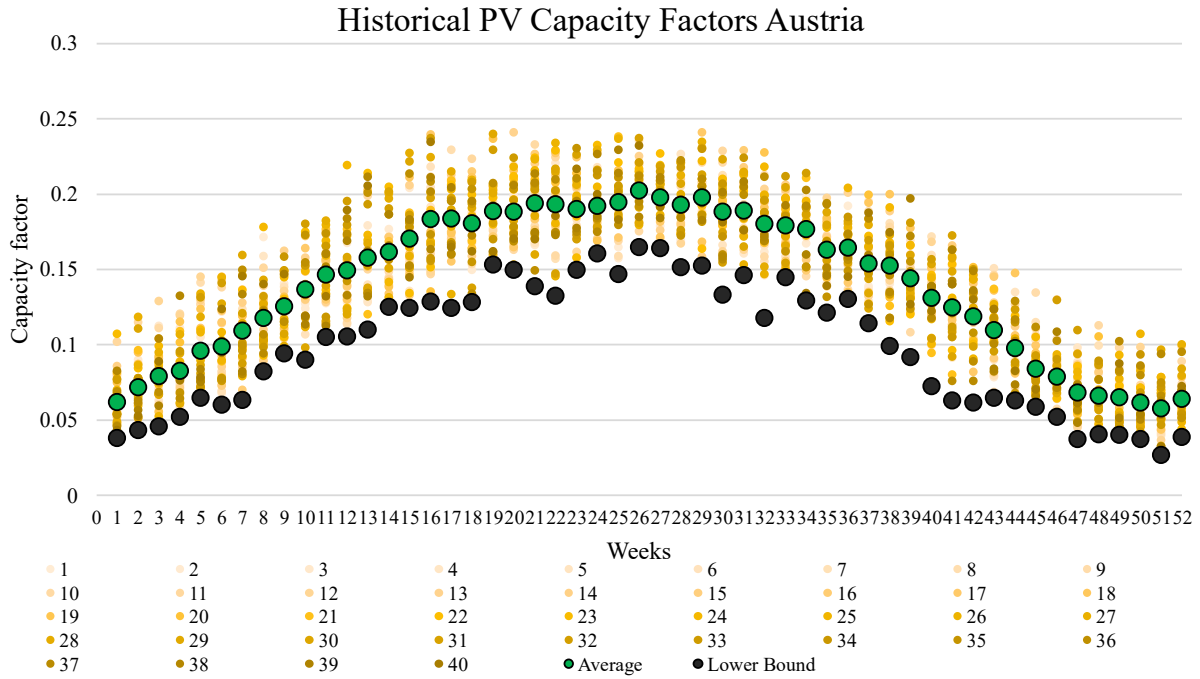


Figure 9: Averaged weekly solar PV capacity factors in Austria, with average weeks in green and lower bounds in black, own illustration.

APPENDIX D

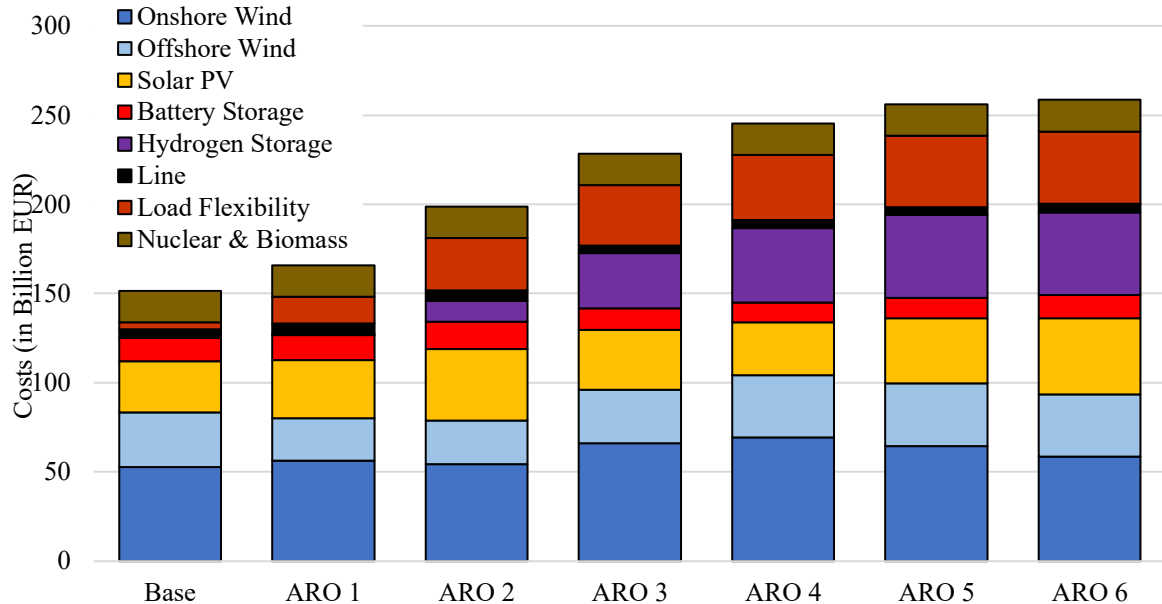


Figure 10. Scenario specific investments and operation costs, own illustration.

Figure 10 shows the costs per scenario differentiated by generation, storage and transmission technology. As we are analyzing a carbon neutral future electricity system, the majority of the costs originate from investments in renewable generation technologies. In the base scenario (left column), wind onshore is the preferred investment, with total investment over Europe amounting to around € 50 bn. Wind offshore and solar PV follow with costs of around € 30 bn each. About € 10 bn is invested in battery storage, smaller amounts in line extensions, biomass, and nuclear operation. The base scenario does not invest in

long term hydrogen storage technologies. Increasing the uncertainty budget, i.e. moving from ARO1 to ARO6 in the graph, we can now deduce which technologies are covering the low wind and solar availabilities. Up to ARO3, the total installed capacity of RES (onshore wind, offshore wind and solar) increases. Additional capacity (MW) thus compensates for reduced availability (MWh per MW). Furthermore, investment shifts to regions which are not affected by reduced renewable availability. From ARO3 to ARO6, aggregated RES capacity remains relatively constant because increasingly more regions are affected by reduced availability. This is because expanding or reallocating renewable capacity becomes less effective in mitigating the impact. Instead, the model prioritizes the increasing use of load shedding and invests in seasonal hydrogen storage. In contrast, the share of battery storage remains almost constant from the ARO3 scenario, because it cannot contribute to shift energy beyond the daily balancing use of residual loads. The same applies to grid expansion, although at significantly lower investment levels.

APPENDIX E

Figure 11 below plots the expanded capacity for each region differentiated between the cross regional capacity and the regional (internal) transmission capacity. Additionally, it presents the import-export balance of the individual regions during the extreme event period. The figure shows that the slightly lower total transmission capacity in the ARO3-ARO6 scenarios originates from the reduced internal transmission line expansion in Region 6. Furthermore, the figure reveals that most cross-border capacity is built in Region 3 and Region 6. This is in line with the corresponding energy exchange between these regions, where Region 3 is a clear exporter and Region 6 a clear importer during all scenarios as indicated by Figure 6.

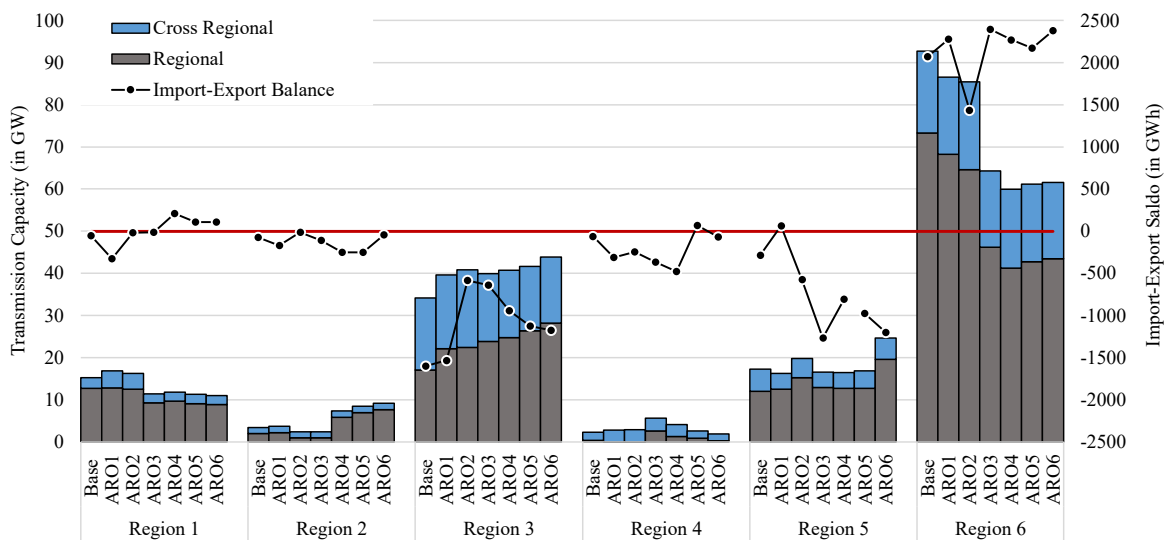


Figure 11: Transmission capacity expansion and import-export balance during extreme event period (January), own illustration.

The dominating importing region throughout all scenarios is Region 6. This result is driven by two factors. The renewable availability on the one hand, and the demand centers on the other hand. Region 6 has the highest electricity demand and comparably poor renewable generation potentials compared to the other regions. Furthermore, the share of the firm capacity (exogenous hydro, biomass, and nuclear power), is the smallest compared to the overall demand. This is leading to a system layout, where Region 6 imports cheaper renewable electricity generated in neighboring regions with a better renewable potential such as Region 1, Region 3, and Region 5.

We also find that depending on the modeled extreme event, Region 6 is influencing the capacity and generation mix in its neighboring regions. For example, while Region 3 is utilizing offshore wind in the Base scenario, it switches to onshore wind generation in the ARO scenarios. In contrast, Region 6 builds more offshore wind capacity. The system seeks to minimize the distance between generation and demand centers: onshore wind is now prioritized in Region 3 due to its proximity to Region 6, while offshore wind is favored in Region 6 because, even during low wind availability events, offshore wind has greater generation potential than onshore wind.

APPENDIX F

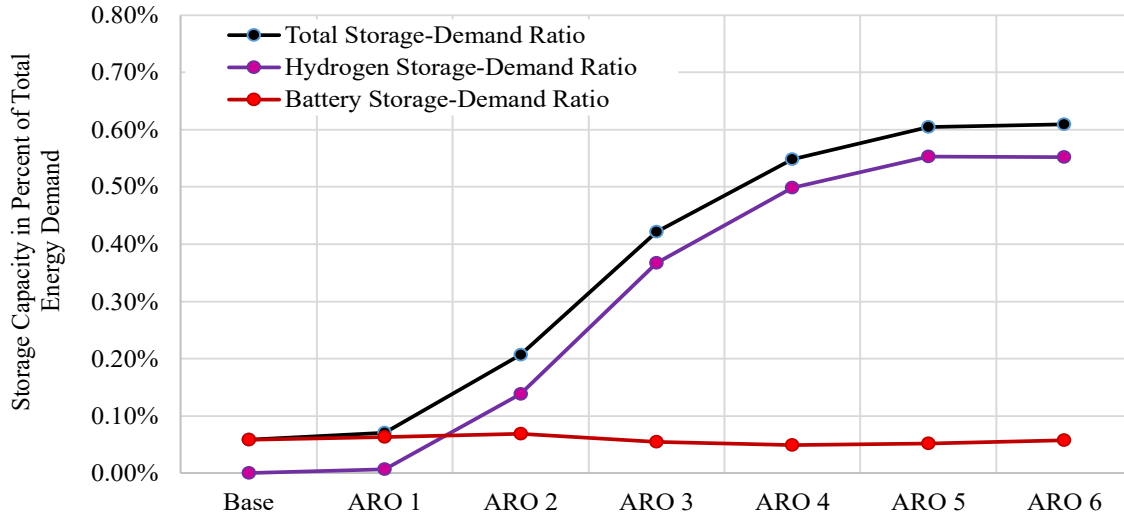


Figure 12: Scenario and technology specific storage capacity demand ratio, own illustration.

Figure 12 shows that the total storage-demand ratio falls between 0.08 % for the Base and 0.7 % for the ARO6 scenario, which is in line for estimates for 100% renewable systems Zerrahn et al. (2018). The ratio significantly increases from scenario ARO2 onwards. This increase is related to the expansion of long-term hydrogen storage. The hydrogen storage capacity increases strongly in the ARO2 to ARO4 scenarios compared to the Base scenario while it is the same in ARO5 and ARO6. On the contrary, the battery storage capacity remains almost constant throughout all scenarios.

The regional specific energy storage to demand is depicted in Figure 13 below. The figure shows that Region 1, Region 3 and Region 5 proportionally drive the storage expansion the most.

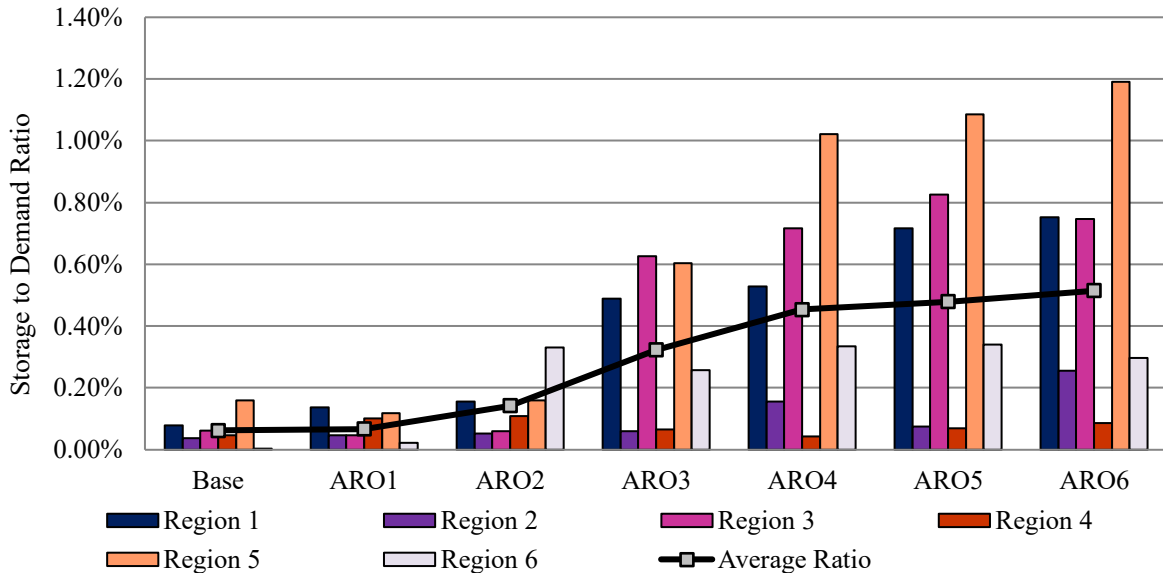


Figure 13: Scenario specific regional comparison of storage capacity to demand ratio.

APPENDIX G

Figure 14 illustrates the convergence process for each ARO scenario, with the duality gap plotted on a logarithmic scale (y-axis) over the number of iterations (x-axis). The red line indicates the convergence tolerance that serves as the stopping criterion for the algorithm.

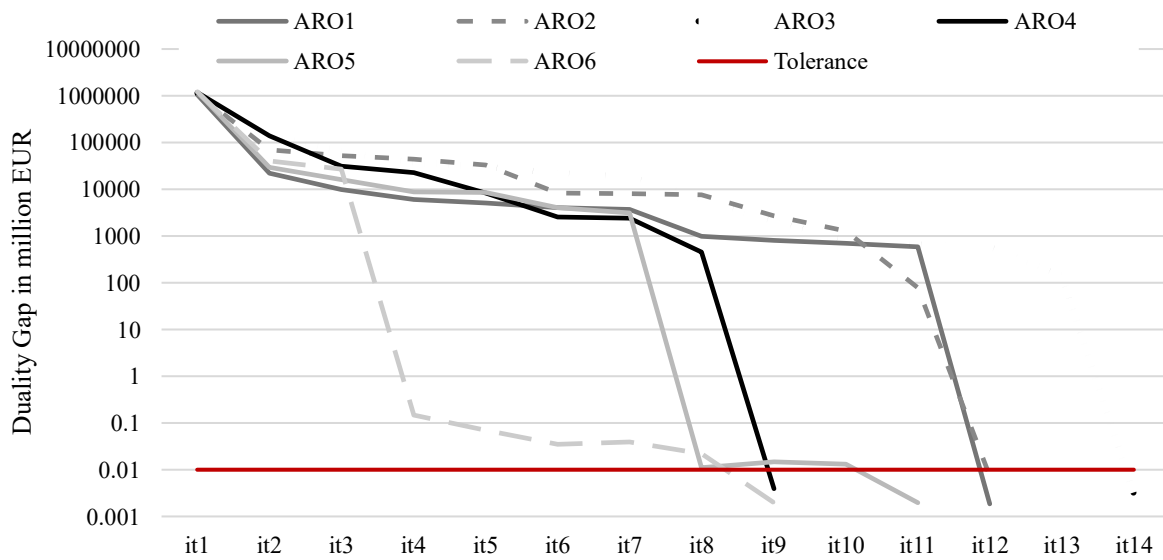


Figure 14: Convergence Process - Development of the Duality Gap for each ARO Scenario

The figure reveals a consistent three phase convergence progress of the ARO algorithm. In the first phase, the algorithm rapidly minimizes the duality gap up to a certain cost interval between 100 billion and 10 billion EUR. From here the second phase can be seen as saturation phase, where the min-max algorithm slowly progresses on closing the duality gap. In the third and final phase, a steep decline in the duality gap is observed, reflecting the identification of near-robust or robust capacity layout that meets the convergence criterion. As one can see, this process is different for each ARO scenario. Scenarios such as ARO1, ARO2, and ARO3 require more iterations to converge. This indicates that identifying a robust system layout in these cases requires exploring a broader set of adverse weather events before achieving convergence. The resulting extreme event realization in the last iteration is then referred to as the worst-case geographical configuration within the given uncertainty budget.